National Aeronautics and Space Administration

COMBINED ANNUAL STATUS REPORT &

FINAL TECHNICAL REPORT FOR NAG 5-1606

Prepared by:

Columbia Astrophysics Laboratory
Departments of Astronomy and Physics
Columbia University
538 West 120^{th} Street
New York, New York 10027

Submitted by:

The Trustees of Columbia University
in the City of New York
Box 20, Low Memorial Library
New York, NY 10027

Titles of Research:

(1) Imaging the Nearby Seyfert 2 Galaxy NGC 1068

(2) Intermediate Type Seyfert Galaxies

(3) Spectrum and Variability of Geminga

Principal Investigator:

Jules P. Halpern
Columbia University

Period Covered by Report: 1 June 1991 – 31 December 1992

11 January 1993

TABLE OF CONTENTS

The results of the research for NASA Grant NAG 5-1606 are summarized in the following publications:

A ROSAT HIGH RESOLUTION X-RAY IMAGE OF NGC 1068

J. Halpern, Columbia University, New York, NY 10027

ABSTRACT

The soft X-ray properties of the Seyfert 2 galaxy NGC 1068 are a crucial test of the "hidden Seyfert 1" model. It is important to determine whether the soft X-rays come from the nucleus, or from a number of other possible regions in the circumnuclear starburst disk. We present preliminary results of a ROSAT HRI observation of NGC 1068 obtained during the verification phase. The fraction of X-rays that can be attributed to the nucleus is about 70%, so the "soft X-ray problem" remains. There is also significant diffuse X-ray flux on arcminute scales, which may be related to the "diffuse ionized medium" seen in optical emission lines, and the highly ionized Fe Kα emission seen by BBXRT.

INTRODUCTION

In the hidden Seyfert 1 model of NGC 1068 (Antonucci and Miller 1985), the ionizing flux is seen only indirectly via electron scattering from a warm, ionized medium above the axis of an obscuring molecular torus. The results of spectropolarimetry of the Balmer lines require that the electron temperature in the scattering region is $\leq 3 \times 10^5$ K (Miller *et al.* 1991, hereafter MGM). It is difficult, but not impossible, for soft X-rays to emerge unabsorbed through a gas at this low temperature (Monier and Halpern 1987). Careful fine tuning of the photoionization model is required to avoid imprinting absorption or emission features on the soft X-ray spectrum (MGM). This problem would be avoided entirely if the soft X-rays are *not* coming from the nucleus, a reasonable expectation since NGC 1068 is also a bright starburst galaxy.

RESULTS

A 20,000 s observation of NGC 1068 was obtained with the ROSAT HRI between July 24 and 26, 1990. The observed X-ray luminosity of NGC 1068 in the 0.1 – 2.4 keV band is $\sim 9 \times 10^{41}$ ergs s^{-1} (for a distance of 22 Mpc), consistent with previous measurements. The central region of the HRI image is shown in Figure 1, and an X-ray contour map of the galaxy is shown in Figure 2. There is a "nuclear" source, which is characterized by FWHM = 5″.5 in the east-west direction, and 7″ in the north-south direction. This is close to the theoretical FWHM of 5″ which is expected to result when the effects of mirror and detector resolution, and aspect solution are combined. There is not yet enough calibration data available to test whether the marginal extent in the north-south direction is real. The fraction of X-rays from NGC 1068 that can be attributed to the "nucleus" is about 70%, as indicated by the X-ray flux within a radius of 9″, which is 3 sigmas of the radial Gaussian corresponding to the observed FWHM.

There is also significant diffuse X-ray flux on an arcminute scale. It covers much of the galaxy, and is elongated at position angle $\sim 35°$, which is similar to that of the nuclear radio structure (Wilson and Ulvestad 1983). The surface brightness is greatest in the northeast, which is the direction of the one-sided ionization cone (Pogge 1988) and the region of strong, high-excitation [Ne V]

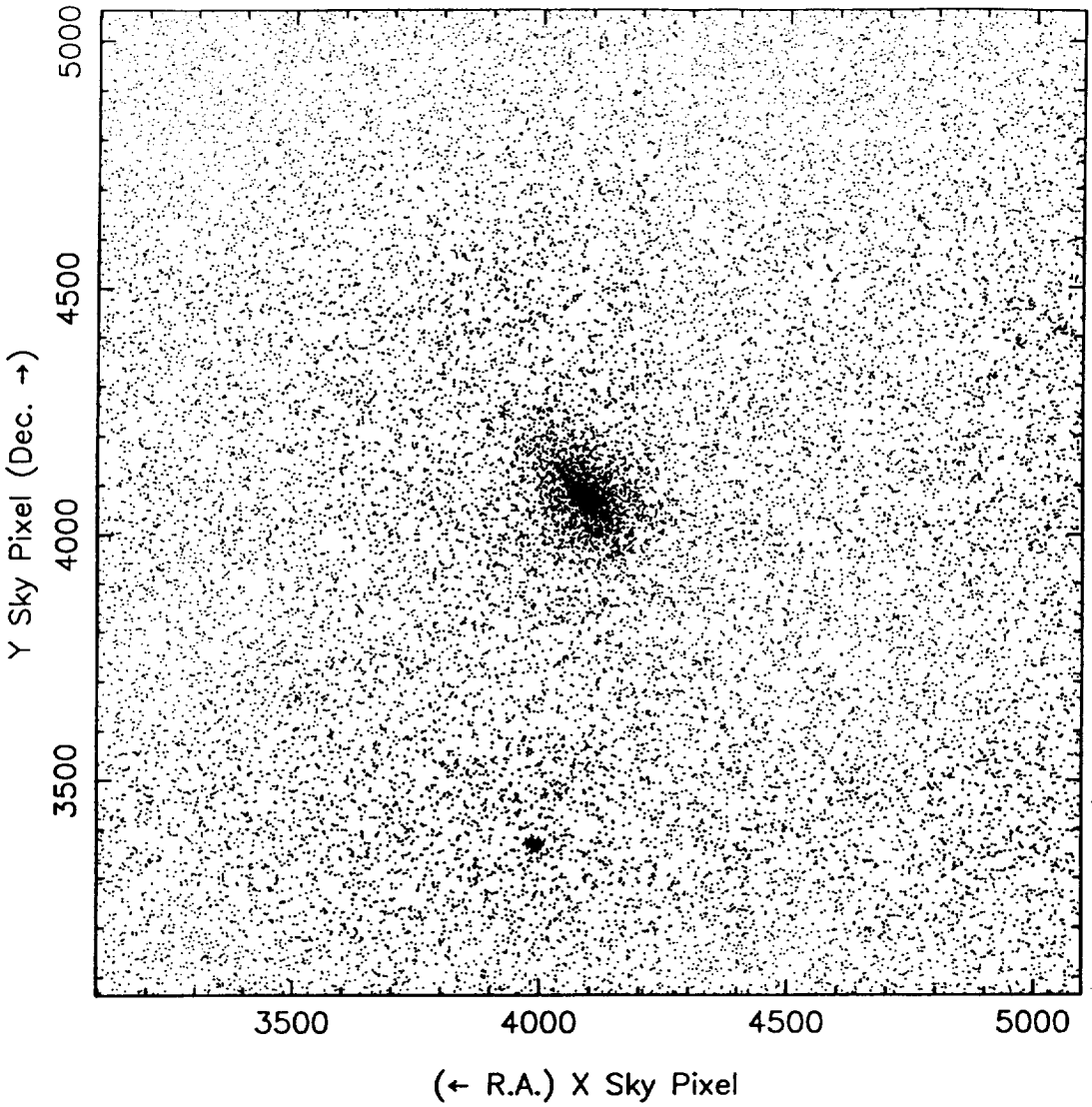

FIG. 1. – The ROSAT HRI image of NGC 1068, showing the central $16'.7 \times 16'.7$ of the field. Each dot represents one photon. Approximately 11,700 photons are detected in a region of radius $2'$ centered on NGC 1068, of which $\sim 70\%$ can be attributed to the nucleus. A stellar source is also detected $5'.8$ south of the galaxy.

λ3426 emission (Evans and Dopita 1986; Bergeron *et al.* 1989). In the northeast direction, the diffuse X-ray emission extends as far as the large-scale 20 cm radio emission of the disk (Wilson and Ulvestad 1982). The diffuse luminosity within a $1'$ radius (6 kpc) is $\sim 4 \times 10^{41}$ ergs s^{-1} when corrected for Galactic $N_H = 3 \times 10^{20}$ cm^{-2}, which is comparable to that of other bright starburst galaxies (Ward 1988). Similar luminosities of extended X-ray emission were detected in *Einstein* HRI images of several Seyfert 1 galaxies (Elvis *et al.* 1990). In NGC 1068, about 20% of the total X-ray flux comes from a region which is larger than the $30''$ diameter starburst disk.

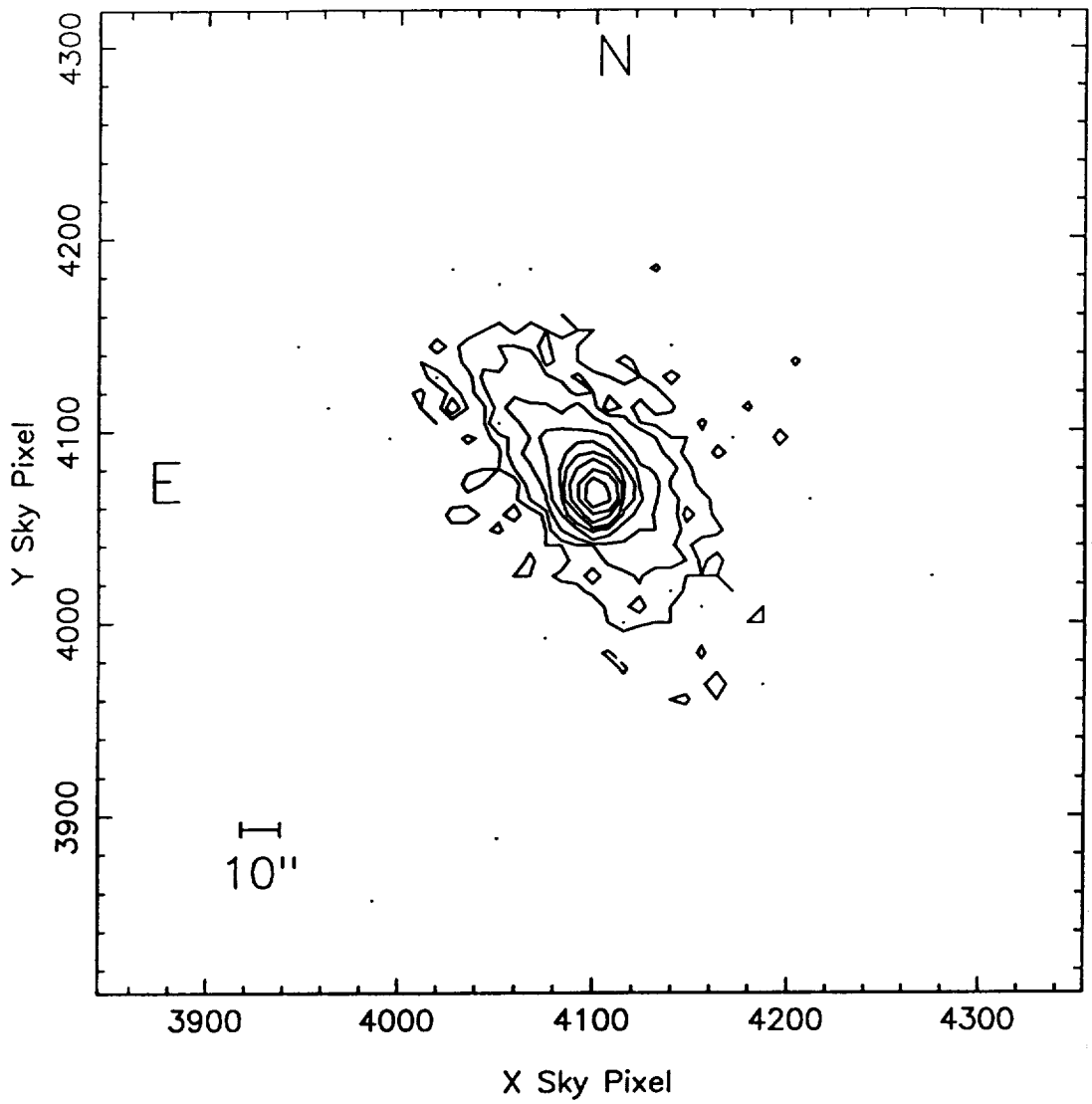

FIG. 2. – Contour map of the X-ray image of NGC 1068. The field is $4' \times 4'$. The image has been binned into $4'' \times 4''$ pixels. The lowest contour level corresponds to an intensity of 4 counts per pixel, or a flux of $\sim 1.5 \times 10^{-14}$ ergs cm^{-2} s^{-1}. The contour levels are separated by factors of 2 in intensity.

INTERPRETATION

The detection of a nuclear soft X-ray source, in combination with the lack of oxygen features in the BBXRT spectrum (Marshall 1992), presents a significant challenge to the electron scattering model. The emergent X-ray spectrum should have either a K-edge of O^{+7} at 870 eV (Monier and Halpern 1987), or a Lyα recombination line at 654 eV, neither of which are seen (Marshall 1992). One can wriggle out of the problem by noting that the "nuclear" HRI source, with its instrumental resolution of 500 pc, may still be outside the scattering region, for which the theory of MGM favors only a lower limit of 30 pc.

The diffuse X-ray flux is similar in extent to the "diffuse ionized medium" seen in the [N II] and Hα imaging Fabry-Perot data of Bland-Hawthorn *et al.* (1991). Unlike H II regions, the ratio [N II] λ6584/Hα is greater than 1. The large velocity widths of the lines in comparison with the adjacent H II regions, led these authors to predict that the scale height of the emitting filaments might be high, $\sim$ 400 pc, and that they might be confined by, or condense out of, a hot phase which would be seen by ROSAT. The HRI image is substantially in agreement with this prediction. Since some of the X-ray flux comes from a region which is larger than the 30″ diameter starburst disk, it is likely to originate in a diffuse hot medium, rather than numerous discrete supernova remnants or binary X-ray sources. To explain the diffuse X-ray emission as bremsstrahlung at $T \sim 10^7$ K, we require emission measure $n_e^2 V \sim 7 \times 10^{64}$ cm^{-3}, or electron density $n_e \sim 0.15$ over the inner 6 kpc radius and 400 pc scale height. This medium would also be responsible for the He and H-like iron lines seen the in BBXRT spectrum, which requires $n_e^2 V \sim 1.5 \times 10^{64}$ cm^{-3} at $T \sim 10^7$ K (Marshall 1992). It could also exist in pressure balance with optical filaments of density ~ 100 cm^{-3} and filling factor $\sim 10^{-6}$.

The cooling rate of the optical filaments is estimated to be $\sim 4 \times 10^{42}$ ergs s^{-1} (Sokolowski *et al.* 1991), while the diffuse X-ray luminosity is ten times smaller. Photoionization by the active nucleus is an ample source of energy for both the optical filaments and the X-ray emitting gas, although the ionization parameter may not be high enough to heat the low-density medium to 10^7 K. In the context of the the obscuring torus/electron scattering model, the *intrinsic* ionizing luminosity L of the nucleus is related to the *observed* luminosity L_o via $L = (1/\tau_{es})(4\pi/\Omega)L_o$, where Ω is the unobscured solid angle. Estimates of L range between 7×10^{43} and 1×10^{45} ergs s^{-1} (Monier and Halpern 1987; Sokolowski *et al.* 1991), or even higher if there is intrinsic beaming (MGM). So the diffuse optical filaments need only absorb $\sim 1\%$ of the nuclear luminosity to power the emission lines. However, the ionization parameter ($\xi = L_x/nr^2$) must be ~ 1000 in the X-ray emitting medium for He and H-like iron to predominate. This can only occur if the nuclear luminosity is $\geq 10^{45}$ ergs s^{-1}, as estimated by MGM. Alternatively, shock heating by supernova remnants or energetic stellar winds may contribute to the energetics of the diffuse X-ray emitting gas.

REFERENCES

Antonucci, R. R., and Miller, J. S. 1985, *Ap. J.*, **297**, 621.
Bergeron, J., Petitjean, P., and Durret, F. 1989, *Astr. Ap.*, **213**, 61.
Bland-Hawthorn, J., Sokolowski, J., and Cecil, G. 1991, *Ap. J.*, **375**, 78.
Elvis, M., Fassnacht, C., Wilson, A. S., and Briel, U. 1990, *Ap. J.*, **361** 459.
Evans, I. N., and Dopita, M. A. 1986, *Ap. J. (Letters)*, **310**, L15.
Marshall, F. E. 1992, this volume.
Miller, J. S., Goodrich, R. W., and Mathews, W. G. 1991, *Ap. J.*, **378**, 47 (MGM).
Monier, R., and Halpern, J. P. 1989, *Ap. J. (Letters)*, **315**, L17.
Pogge, R. 1988, *Ap. J.*, **328**, 519.
Sokolowski, J. K., Bland-Hawthorn, J., and Cecil, G. 1991, *Ap. J.*, **375**, 583.
Ward, M. J. 1988, *M.N.R.A.S.*, **231**, 1P.
Wilson, A. S., and Ulvestad, J. S. 1982, *Ap. J.*, **263**, 576.
Wilson, A. S., and Ulvestad, J. S. 1983, *Ap. J.*, **275**, 8.

Discovery of soft X-ray pulsations from the γ-ray source Geminga

J. P. Halpern* & S. S. Holt†

* Columbia Astrophysics Laboratory, Columbia University, 538 West 120th Street, New York, New York 10027, USA
† Director of Space Sciences, Code 600, NASA Goddard Space Flight Center, Greenbelt, Maryland 20771, USA

THE nature of the γ-ray source 'Geminga' (2CG195+04) is a problem of considerable importance in high-energy astrophysics. First discovered in 1972 by the SAS-2 satellite[1], Geminga emits virtually all its power at energies above 50 MeV, and at energies above 100 MeV is the second brightest source in the γ-ray sky survey made by the Cos-B satellite[2]. It eluded identification at all other wavelengths until the Einstein Observatory found an unusual soft X-ray source, 1E0630+178, in its error box[3]. This source also has a claimed twenty-fifth magnitude optical counterpart[4–6]. This distinctive set of properties is reminiscent of the Vela pulsar, except for the absence of radio emission[7] or a synchroton nebula[3]. We have made a more sensitive soft X-ray observation of the Geminga field using Rosat, and have detected coherent pulsations from 1E0630+178 at a period of 0.237 s. This result confirms suggestions[3–6,8,9] that Geminga is, like Vela, a γ-ray pulsar. We speculate that Geminga is somewhat the older of the two. With this discovery we consider the mystery of Geminga largely solved.

For Geminga, the soft X-ray band is the most promising one for a pulsar search because the count rate is high and the background is negligible. The Geminga field was observed with the Position Sensitive Proportional Counter (PSPC) aboard Rosat[10] during 1991 March 14–17. A total of 14,390 s of exposure were obtained during 10 satellite orbits as listed in Table 1. The mean count rate of 1E0630+178 was 0.53 s^{-1} in the 0.07–2.4-keV band. A total of 7,630 counts were detected within a circle of radius 1.5′ about the source centroid, of which only ~1% are background. After transforming the photon arrival times to the barycentre of the Solar System using the accurate (~3″) Einstein High Resolution Imager position, the search for periodicity was begun by performing a fast Fourier transform (FFT) on the section of data consisting of four consecutive orbits on March 16. The FFT covered 262,144 independent trial periods down to a minimum period of 0.072 s. The only significant peak in the power spectrum occurred at a period of 0.237097 s, for which the power is 17.5 times the mean. The probability that a peak of this strength or greater will occur by chance somewhere in the power spectrum is 0.007. The same section of data was then folded about a range of trial periods. The χ^2 values of the resulting five-bin folded light curves were calculated with respect to a constant mean. The candidate period appeared with $\chi^2 = 39.5$ for 4 degrees of freedom. The probability that χ^2 greater than or equal to this value will occur by chance in a single trial is 6×10^{-8}. When multiplied by the number of trial periods, the chance probability is 0.016. The highest χ^2 in the periodogram of the folded data is 54.7 (Fig. 1*b*). The single-trial chance probability is less than 10^{-10}, but the effective number of periods searched in the epoch folding is about a factor of 5 higher than in the FFT. We conclude that the probability that the period is spurious is $\leq 1\times10^{-4}$.

TABLE 1 Rosat observations of Geminga

Date (UT)	Start time (s)	Duration (s)	Counts
1991 March 14	76,564	1,193	612
1991 March 15	1,191	1,437	749
1991 March 15	29,362	1,360	703
1991 March 15	64,656	1,567	866
1991 March 15	76,468	1,272	641
1991 March 16	64,514	1,690	887
1991 March 16	69,999	1,959	1,038
1991 March 16	76,448	1,272	724
1991 March 16	81,745	1,509	786
1991 March 17	46,703	1,131	624

The reality of the signal at 0.237 s is further supported by its presence in the remaining half of the data which was not included in the original FFT. Figure 1*a* shows the periodogram for the five orbits of data obtained on March 14–15. The period is clearly indicated in this independent set of data, although the less-than-optimal sampling introduces many more aliases at the 96-min satellite orbital period and its multiples. Figure 1*c* is the result of the coherent folding of data from all 10 orbits. The

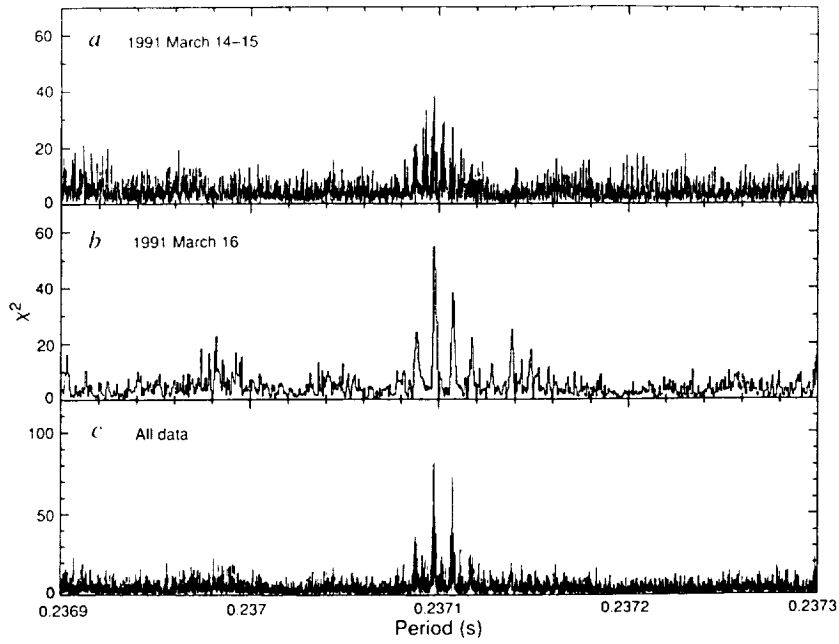

FIG. 1 Periodograms of the five-bin folded light curves. The multiple peaks are aliases of the 96-min satellite orbital period. The best-fit period is 0.2370974 s±0.1 μs.

highest peaks in all three panels are at the same period to within the errors. The symmetry of the peak structure indicates that the highest peak at 0.2370974 s ± 0.1 μs is most likely to be the true period. In addition to these analyses, the period is detected weakly in those individual orbits having more than 1,500 s of exposure. There is no evidence for orbital motion or a secular change in period P during the span of these observations. On a timescale of two days, the upper limit on $\dot{P}$ is 2×10^{-12} s s^{-1}, and Δv is less than 0.5 km s^{-1}. We conclude that the 0.237-s period is not an instrumental artefact, because similar analyses on background counts collected at different positions in the detector do not reveal a signal. We do not detect a significant signal at any other period, including previously reported periods[11-13] near 60 s, even though the PSPC is at risk of manufacturing spurious periods between 30 and 400 s because of the deliberate dithering of the satellite.

Figure 2 shows the folded light curve in three different energy bands, and their sum. The pulse profile has a single broad peak, which is consistent with the absence of power at submultiples of the 0.237-s period. The pulsed fraction is 24% in the band 0.07–0.2 keV and declines with energy. At 0.2–0.28 keV, the pulsed fraction is 19%, and at 0.28–1.50 keV it is 15%. These pulsed fractions are probably lower limits, as there is a known timing error in the processed data which shifts some of the photon arrival times randomly with respect to the phase of the 0.237-s period. The extremely soft spectrum of the pulsations, and the broadness of the pulse profile, are suggestive of thermal emission from the surface of a neutron star. But it is difficult to interpret these data in terms of surface temperature and distance, because the X-ray spectrum in the Rosat bandpass can be modified from the black-body shape as a result of non-grey atmospheric opacity[14]. Strong L and K edges could be present. Rosat has recently detected soft X-ray pulsations from Vela[15], also in the lowest energy channels.

To study the X-ray spectrum, we extracted all the source counts within a 2′ radius, and subtracted background from an annulus between radii of 2.5′ and 4.2′. The total flux in the 0.1–2.4-keV band is $\sim1.5\times10^{-12}$ erg cm^{-2} s^{-1}, which is roughly consistent with the Einstein result. The X-ray spectrum is very soft, but it cannot be adequately fitted by a black-body or a power-law spectrum, as illustrated in Fig. 3. We have not yet explored the full range of plausible spectral models, but with the caveat concerning atmospheric opacity in mind, a composite model consisting of a black body of temperature $T\approx(3-4)\times10^5$ K plus a power-law component with energy index α in the range 0.75–1.75 yields an adequate fit to the data. In

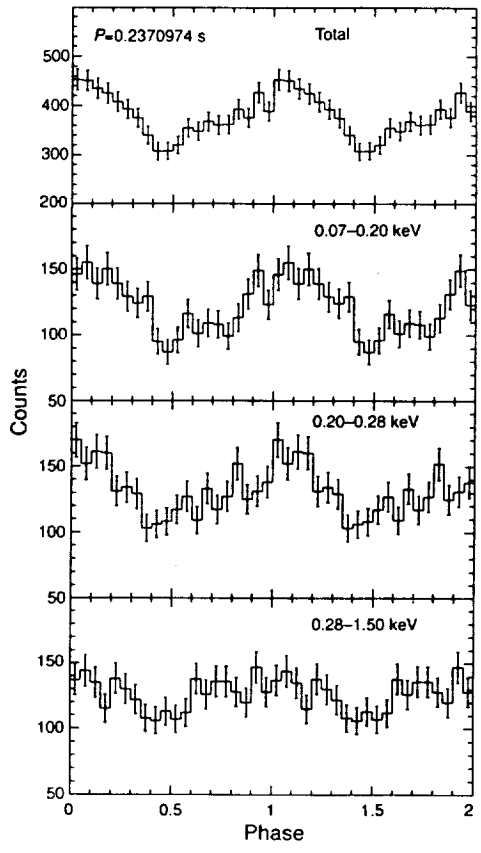

FIG. 2 Pulse profile of all data between 0.07 and 1.5 keV folded into a 20-bin light curve. The top panel is the sum of the bottom three. ►

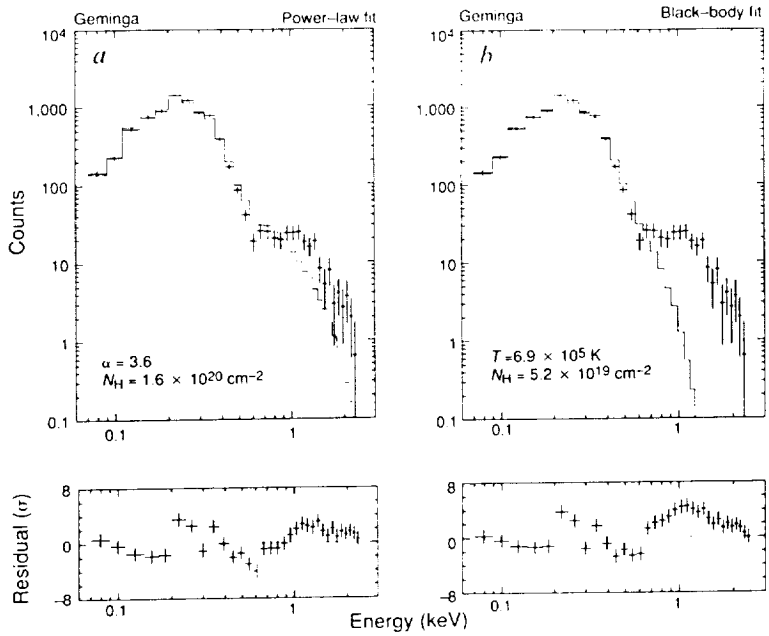

FIG. 3 Spectral fits with single-component models. *a*, Power law; *b*, black body.

this model, the decrease of pulsed fraction with energy might be caused by the increasing contribution of an unpulsed synchrotron component. A column density in the range $(0.5\text{–}3)\times 10^{20}\,\mathrm{cm}^{-2}$ is allowed.

Observations indicating that Geminga might be a pulsar somewhat older than Vela have been reviewed previously[3–6,8]. The overall energy distributions of the two objects are similar at wavelengths from optical through γ-rays. The ratio $L_\gamma/L_x = 1{,}000$ is a likely indicator of a pulsar emission mechanism. The ratio $L_x/L_{opt} \approx 1{,}800$, and the soft X-ray spectrum, also suggest an isolated neutron star. The discovery of a short pulse period fulfils this expectation. A detailed theoretical model for γ-ray pulsars was developed by Ruderman and Cheng[9], who proposed an evolutionary scheme in which a short-period γ-ray pulsar evolves from a Crab-like stage, through that of Vela, and finally reaches that of Geminga. In the regime of Vela-like pulsars, γ-rays are produced in the outer magnetosphere as synchrotron radiation from electron-positron pairs. As it slows down, such a pulsar uses an ever increasing fraction of its spin-down power in the production of an $e^\pm$ wind and associated γ-ray emission until almost the full spin-down power, $\sim 4\times 10^{36}\,\mathrm{erg\,s}^{-1}$, goes into this mechanism. As the period increases further, the currents necessary to sustain pair production are quenched and the γ-ray emission ceases. They predicted that Geminga is near the turnoff period, which for Vela itself would be ~0.13 s, and postulated that ordinary pulsars avoid this fate because they have more highly curved magnetic field lines near the polar cap, which can maintain the potential drop required for pair production.

The theory was generalized by Chen and Ruderman[16], who argued that there is actually a death line for Vela-like (outer gap) pulsars given by $5\log B - 12\log P = 72.2$, where B is the surface magnetic field. If Geminga is to fall near this line, it must have $B \approx 1\times 10^{13}$ G, only a factor of 3 greater than that of Vela. In this case, the total spin-down power, $\dot{E} \approx B^2R^6\Omega^4/c^3$, would be $\sim 1.8\times 10^{36}\,\mathrm{erg\,s}^{-1}$. As the observed γ-ray flux[1] is at least $2.4\times 10^{-9}\,\mathrm{erg\,cm}^{-2}\,\mathrm{s}^{-1}$, an upper limit to the distance is $2{,}500\,(B/10^{13})$ pc for the luminosity not to exceed the estimated spin-down power. (The column density derived from the X-ray spectrum almost certainly restricts the distance to less than 500 pc.) The predicted magnetic field would result in a spin-down rate of $4\times 10^{-13}(B/10^{13})^2\,\mathrm{s\,s}^{-1}$, significantly below the upper limit of 2×10^{-12} established by this observation. A second observation could easily determine $\dot{P}$, and thus the magnetic field. The fact that Geminga is not detected in high-energy X-rays or low-energy γ-rays[17] is consistent with the outer gap model. The low-energy cutoff of the spectrum at a frequency ω_c is determined by the energy of the $e^\pm$ pairs that leave the magnetosphere before losing their energy to synchrotron radiation. Because $\omega_c \propto \Omega^{-7}B^{-3}$, scaling from the Vela break at ~1 MeV (ref. 7) predicts a break at ~25 MeV for Geminga. Other pulsars that may be progenitors of the Geminga-like γ-ray pulsars are PSR1509−58 (ref. 18) with $P = 0.150$ s and PSR1706−44 with $P = 0.102$ s. These both fall in the region of Vela-like pulsars[16], and were recently detected[19,20] by the Compton Gamma Ray Observatory (CGRO).

Our results thus largely confirm the expectation that Geminga is a pulsar similar to Vela. The absence of a synchrotron nebula around Geminga remains a fundamental difference, which is perhaps related to the fact that Geminga has the longest period of the γ-ray pulsars. We suggest that many of the other unidentified high-energy γ-ray sources are spinning neutron stars which are 'radio quiet', or whose radio beams do not intersect the Earth. Rosat should be able to identify γ-ray pulsars by finding the periods of sources detected by CGRO in the galactic plane. □

Received 30 March; accepted 28 April 1992.

1. Fichtel, C. E. *et al. Astrophys. J.* **198,** 163-182 (1975).
2. Swanenburg, B. N. *et al. Astrophys. J.* **243,** L69-L73 (1981).
3. Bignami, G. F., Caraveo, P. A. & Lamb, R. C. *Astrophys. J.* **272,** L9-L13 (1983).
4. Bignami, G. F. *et al. Astrophys. J.* **319,** 358 (1987).
5. Halpern, J. P. & Tytler, D. *Astrophys. J.* **330,** 201-217 (1988).
6. Bignami, G. F., Caraveo, P. A. & Paul, J. A. *Astr. Astrophys.* **202,** L1 (1988).
7. Spoelstra, T. A. & Hermsen, W. *Astr. Astrophys.* **135,** 135-140 (1984).
8. Halpern, J. P. in *Proc. GRO Science Workshop* (ed Johnson, N.) 4-166-4-173 (1989).
9. Ruderman, M. & Cheng, K. S. *Astrophys. J.* **335,** 306-318 (1988).
10. Trümper, J. *et al. Adv. Space Res.* **2,** 241-249 (1983).
11. Bignami, G. F., Caraveo, P. A. & Paul, J. A. *Nature* **310,** 464-469 (1984).
12. Bignami, G. F. in *The Origin and Evolution of Neutron Stars* (eds Helfand, D. J. & Huang, J. H.) 465-474 (Reidel, Dordrecht, 1987).
13. Caraveo, P. A. & Bignami, G. F. in *The Origin and Evolution of Neutron Stars* 545 (eds Helfand, D. J. & Huang, J. H.) (Reidel, Dordrecht, 1987).
14. Romani, R. W. *Astrophys. J.* **313,** 718-726 (1987).
15. Ögelman, H., Finley, J. P., Aschenbach, B., Trümper, J. & Zimmermann, U. *Bull. Am. astr. Soc.* **23,** 1349 (1991).
16. Chen, K. & Ruderman, M. *Astrophys. J.* (in the press).
17. Bignami, G. F. & Hermsen, W. *A. Rev. Astr. Astrophys.* **21,** 67-108 (1983).
18. Seward, F. D. & Harnden, F. R. H. Jr *Astrophys. J.* **256,** L45-L47 (1982).
19. Wilson, R. B., Finger, M. H., Fishman, G. J., Meegan, C. A. & Paciesas, W. S. *IAU Circ.* No. 5429 (1992).
20. Kniffen, D. A. *et al. IAU Circ.* No. 5485 (1992).

ACKNOWLEDGEMENTS. We thank F. R. Harnden and F. Seward for making the barycentric correction, and for assistance with the data analysis. We thank G. Bignami for his review. This work was supported by NASA through a Rosat guest observer grant.

SOFT X-RAY PROPERTIES OF THE GEMINGA PULSAR

J. P. Halpern & M. Ruderman
Columbia Astrophysics Laboratory, Columbia University
538 West 120th Street, New York, NY 10027

Submitted to *The Astrophysical Journal*

Received 1992 December 30 ; *accepted* _____

ABSTRACT

The *ROSAT* soft X-ray spectrum and pulse profile of the Geminga pulsar are analyzed and interpreted in terms of thermal emission from the surface of the neutron star. The X-ray spectrum appears to consist of two blackbody components with $T_1 = (5.2 \pm 1.0) \times 10^5$ K and $T_2 \sim 3 \times 10^6$ K, respectively. The inferred ratio of surface areas, A_2/A_1, is $\sim 3 \times 10^{-5}$. Both components are highly modulated at the pulsar rotation period, but the harder X-ray pulse is narrower, and leads the main (soft) X-ray pulse by about 105° of phase. The soft X-ray component is interpreted as photospheric cooling of much of the neutron star's surface area, while the small, hot region could be part of the much smaller polar cap heated by energetic particles flowing inward from the magnetospheric accelerator which is responsible for the production of Geminga's γ-rays. Geminga's γ-ray emission is consistent with outer-magnetosphere accelerator models for highly inclined dipoles. These predict the beaming of energetic γ-rays close enough to the star to give copious $e^{\pm}$ production in the stellar magnetic field and a large circumstellar pair density from pair inflow toward the surface. These pairs may quench radio emission, and also reflect most of the hard polar cap X-rays back to the stellar surface by cyclotron resonance scattering. They are then reemitted from that much larger area at the lower temperature T_1. The single-peaked nature of the X-ray pulse and its energy-dependent phase suggest an off-center dipole geometry for the *surface* magnetic field.

Under the assumption that the soft X-ray emission comes from the full surface of a neutron star of radius $R = 10$ km, a distance estimate of (150–400) pc is derived. This range is consistent with the fit interstellar column density of $(1.5 \pm 0.5) \times 10^{20}$ cm^{-2}. Distances less than 150 pc are probably ruled out both by the lower limit on the column density, and also by the requirement that the Rayleigh-Jeans extrapolation of the soft X-ray spectrum not exceed the observed blue flux of the faint optical counterpart. This distance estimate implies that Geminga's efficiency for converting spindown power into γ-rays is near unity, and that there may be significant beaming of the γ-rays as well. These results tend to bolster the prospect that most of the unidentified high-energy γ-ray sources in the Galactic plane are pulsars, some of which may be radio quiet.

Subject headings: gamma rays: sources – pulsars – stars: neutron – X-rays: sources

1. INTRODUCTION

The high-energy γ-ray source Geminga (2CG 195+04, 1E 0630+178) is a radio-quiet pulsar with period $P = 0.237$ s, surface field $B_p \sim 1.6 \times 10^{12}$ G, and characteristic age $\tau = P/2\dot{P} = 3.4 \times 10^5$ yr (Halpern & Holt 1992; Bertsch et al. 1992). Its soft X-ray properties contain a great deal of information about thermal emission from the surface of the neutron star. There are very few pulsars for which the bulk of the soft X-ray emission is demonstrably photospheric, and it is argued here that Geminga is one of the more secure cases. Therefore, it can be used to test theories of neutron star cooling, polar-cap heating, and the effect of the surface magnetic field and environment on the emergent spectrum. Other pulsars for which such surface emission is likely to contribute substantially are PSR 0656+14 (Finley, Ögelman, & Kiziloğlu 1992), PSR 1055–52 (Cheng & Helfand 1983; Brinkmann & Ögelman 1987), and Vela (Ögelman, Finley, & Zimmermann 1992), but Geminga allows the most detailed examination so far of the spectrum and pulse properties of the photospheric emission.

If interpreted as blackbody emission, the X-ray spectrum also provides the only measurement of the distance to Geminga, which is crucial to the determination of the efficiency for turning spindown power into γ-rays. This in turn affects the likelihood that the other unidentified Galactic high-energy γ-ray sources are pulsars. Geminga bolsters the hypothesis that the COS B sources are a population of efficient γ-ray pulsars. The X-ray pulse profile of Geminga is complex and highly modulated, and to the extent that it can be interpreted in terms of the geometry of the magnetic field, it may help in understanding the γ-ray emission mechanism and pulse profile. This paper presents a more comprehensive analysis of the *ROSAT* observation of the Geminga pulsar than was possible in the initial report by Halpern & Holt (1992). Although the data are the same, a number of additional results have been obtained, and the interpretation also incorporates properties of the γ-ray emission.

2. PULSE PROFILE AND TIMING

A more detailed soft X-ray pulse profile was constructed by folding about the revised *EGRET* ephemeris (P and $\dot{P}$) of Mayer-Hasselwander et al. (1992), which is more precise than the original X-ray determination. Table 1 gives the folding parameters which apply to the epoch of the *ROSAT* observation in the Barycentric Dynamical Time (TDB) system. A total of 7,911 counts in the 0.07–1.50 keV band, of which less than 2% are background, were extracted from a circle of radius 150″ in the position sensitive proportional counter. Figure 1 shows a number of details that were not apparent in the original examination of the X-ray data. First, there is apparently a sharp dip in the soft X-ray flux, and possibly significant high-frequency structure, especially on the rising side of the pulse. A revised estimate of the pulsed fraction in the 0.07–0.28 keV band is 33%. Although it appeared in Halpern and Holt (1992) that the pulsed fraction decreases with energy, it is now seen that there is actually a faint but highly modulated pulse at energies around 1 keV which leads the peak of the main X-ray pulse by about 105° of phase. The weakness of the modulation around 0.5 keV is due to the fortuitous superposition of these two out-of-phase components, and it appears that both components are individually highly pulsed in a roughly energy-independent manner. We shall refer to the ~ 0.2 keV X-rays and the ~ 1 keV X-rays as the "soft" and "hard" components respectively. The pulsed fraction of the hard X-rays is $\sim 37\%$, similar to that of the soft X-ray pulse, but the hard pulse is narrower. The dip at phase 0.5 is not apparent in the hard light curve, although the photon statistics here are quite poor. The spectral analysis presented in the next section lends additional support to the interpretation of the pulse profiles as two separate components. In particular, the soft component will be interpreted as emission from the full surface of the neutron star, while the hard X-ray pulse could arise from the heated polar caps.

The relative phasing of the X-ray and γ-ray pulses is of great interest, since the pulse profiles are so different. The best current analysis of the *ROSAT* spacecraft clock leads to the alignment shown in Figure 2. The time of phase 0.0 is given by T_0 in Table 1, which is an extrapolation of the *EGRET* ephemeris over the five-week interval between the *ROSAT*

observation and the first *EGRET* observation. The phase comparison using P and $\dot{P}$ should be accurate to better than 0.01 cycles in the absence of significant timing noise, and is comparable to the accuracy of the *ROSAT* spacecraft clock (Ögelman, Finley, & Zimmermann 1992). [It should be noted, however, that $\ddot{P}$ as given by Hermsen et al. (1992) and Mattox et al. (1992) probably *is* dominated by timing noise or cycle count errors, since the quoted values lead to unreasonably large values of the braking index, 31 and 44, respectively.] Another possible source of uncertainty is the position of Geminga, which could cause an error of ≤ 7 msec (0.03 cycles) in the arrival time at the barycenter if it is off by $\leq 3''$ in right ascension. An error of this magnitude would be expected if the G'' optical counterpart (Halpern & Tytler 1988) is incorrect, or if there is exceptionally high proper motion. The tentative detection of a proper motion of $\simeq 0.''2\ \mathrm{yr}^{-1}$ by Bignami, Caraveo, & Mereghetti (1992) would seem to alleviate both of these concerns. More worrisome is a possible ambiguity of 0.5 s in the interpretation of the times from the *ROSAT* spacecraft clock (Ögelman 1992, private communication), which would result in an error of 0.11 cycles in the phase of the pulse. For now, we tentatively accept the relative phasing of the X-ray and γ-ray pulses shown in Figure 2 as correct to within ~ 0.13 cycles.

The sharp, double-peaked γ-ray pulse is in marked contrast to the broad, single-peaked X-ray pulse. In § 5.2, it is argued that Geminga's high γ-ray efficiency and the 180° separation of its γ-ray peaks call for a highly inclined dipole. If so, the single hard X-ray pulse cannot be understood in terms of polar-cap emission from a dipole close to the center of the star, since both polar caps should be visible with a near 180° separation of their X-ray emission. The soft X-ray component is presumed to come from nearly the full surface of the star, and it too is single-peaked. The simplest resolution of this problem invokes an off-center dipole, as described in § 5.5, so that the polar caps are too close together to be resolved in the light curve of the rotating star. The γ-ray pulses originating in the outer magnetosphere can nevertheless be double fan beams which are visible from most directions. The hard X-ray pulse roughly coincides with the bridge of γ-ray emission between the two main peaks, which is consistent with an off-center dipole configuration if the γ-rays are coming from regions along the open field lines which are roughly symmetric with respect to the polar caps.

3. SPECTRAL ANALYSIS

The X-ray source counts were extracted from a circle of radius 150'', and background from an annulus between radii of 150'' and 250''. A total of 7,637 net counts were detected in the 0.08–2.45 keV band in a live time of 14,205 s. As shown by Halpern & Holt (1992), the spectrum cannot be fitted by a single blackbody or power-law, both of which leave a residual hard excess above 0.6 keV. Two-component models are adequate, and one which is particularly amenable to interpretation is a pair of blackbodies,

$$F(E) = C\,E^3 \left(\frac{1}{e^{E/kT_1} - 1} + \frac{f}{e^{E/kT_2} - 1} \right) e^{-\sigma(E) N_{\mathrm{H}}} \ \mathrm{keV\,cm^{-2}\,s^{-1}\,keV^{-1}}. \qquad (1)$$

The interstellar medium photoelectric cross sections of Morrison & McCammon (1983) are used for $\sigma(E)$. The four fitting parameters are the temperatures T_1 and T_2, interstellar column density N_{H}, and fraction f which is closely related to the ratio of surface areas (A_2/A_1) of the two blackbody components. (For each trial spectrum, the normalization constant C is fixed by the total counts, and its error is largely systematic.) A full four-dimensional χ^2 grid search was performed, and the best fit is shown in Figure 3.

Before interpreting these results, it is necessary to point out that there are a number of sharp features in the residuals between 0.2 and 0.4 keV which have been seen in other sources, and which are thought to reflect an as yet unsolved problem in the pulse-height analysis or the detector response matrix. These features are not all likely to be real, and they contribute to an unacceptable total χ^2 of 61 for 42 degrees of freedom. In the hope that the overall continuum

shape is not significantly affected by this problem, a simple renormalization of the χ^2 values by the factor 42/61 was made to permit sensible confidence contours to be derived.

A number of interesting results can be drawn from this fit. First, the relative contributions of the two blackbodies cross over at ~ 0.6 keV, which is very close to the energy of minimum modulation as seen in the light curve (Figure 1). This coincidence lends additional credence to the idea that two components are present in the X-rays, since they can be separated both spectrally and temporally. The lower temperature blackbody with $T_1 \simeq 5 \times 10^5$ K accounts for about 96% of the bolometric flux, and its fit is relatively insensitive to the presence of the weaker hard component. If the χ^2 grid is projected onto the $(T_1, N_{\rm H})$ plane, the confidence contours shown in Figure 4 restrict the temperature and column density to the ranges $(3-6) \times 10^5$ K and $(1-3) \times 10^{20}$ cm^{-2}, respectively. The confidence contours are elongated because the errors on T_1 and $N_{\rm H}$ are correlated. Further restrictions on these parameters are made possible by the incorporation of optical data as described in § 4 below.

A second interesting projection of the χ^2 grid is onto the (T_2, f) plane. Figure 5 shows that T_2 lies in the range $(2.3-3.9) \times 10^6$ K, and that the fractional area f is $\sim 3 \times 10^{-5}$. The very large range allowed for $f, 10^{-6} - 10^{-4}$, is dominated not by the uncertainty in the flux of the hard component, but rather by the ranges in $N_{\rm H}$, T_1, and normalization of the soft component since a large and uncertain fraction of the soft emission is absorbed in the intervening interstellar medium. Projections of the corresponding best fit values of T_1 are shown as dashed lines in Figure 5. A summary of the best fit spectral parameters is given in Table 2. The hard component is interpreted in § 5.3 in terms of polar-cap heating of an off-center dipole by an outer magnetosphere accelerator. A division of the pulse height spectrum into several time-resolved segments according to rotation phase demonstrates that each of the two components varies in an approximately energy independent manner. That is, no variations in T_1 or T_2 are detectable as a function of rotation phase, although the paucity of counts above 0.5 keV precludes a meaningful test for variation in T_2.

A second not implausible two-component model of the X-ray spectrum consists of a blackbody plus a power law,

$$F(E) = C \left(\frac{E^3}{e^{E/kT_1} - 1} + f\, E^{-\alpha} \right) e^{-\sigma(E) N_{\rm H}} \ \ {\rm keV\,cm^{-2}\,s^{-1}\,keV^{-1}}, \qquad (2)$$

where α is the energy index. The best fit spectrum is shown in Figure 6, and the parameters and uncertainties are listed in Table 3. The fit is nearly as good ($\chi^2 = 63$) as the double blackbody. Since the power-law component makes a small contribution to the total X-ray flux, the fit parameters for the soft blackbody are not significantly different from those in the double blackbody model. Although the best fit T_1 is changed slightly, the confidence contours encompass the same range of parameters, as shown in Figure 7. An extrapolation of the power-law component with $F(E) \propto E^{-1.5}$ to the visible would exceed the flux of the 25 mag G″ optical counterpart (Halpern & Tytler 1988) by a factor of several hundred. If the hard component were to be interpreted as synchrotron emission from the magnetosphere, the local magnetic field must be such that the low-frequency cutoff at $\omega = eB/mc$ lies above the optical band. This implies that $B > 10^9$ G. Therefore, any X-ray synchrotron emission would have to arise from within 10 stellar radii of the surface of the neutron star. Synchrotron self-absorption is not an alternative explanation for the weakness of the optical emission, since $\nu_{\rm abs} < 10^{13}$ Hz for this component. Although formally acceptable, a synchrotron origin for the hard X-rays seems less attractive than surface emission because it is difficult to understand why magnetospheric emission far from the stellar surface should have a single-peaked pulse. Regardless of the nature of the hard X-rays, the weak optical flux *could* be synchrotron emission coming from radii *larger* than 10^7 cm. The optical flux in the visible band is only 1.7×10^{-15} ergs cm^{-2} s^{-1}, which is a factor of 100 less than that of the "hard" X-ray component at 1 keV.

4. DISTANCE TO GEMINGA

The softer X-ray component currently provides the only measurement from which the distance to Geminga can be inferred. Several constraints on the distance are associated with the spectral fit. For each point in Figure 4, the normalization constant C can be converted to a visual magnitude by extrapolation of the Rayleigh-Jeans tail of the X-ray spectral fit. If we assume in addition that the X-ray emission comes from the full surface of a neutron star of radius $R = 10$ km, then a distance can be assigned to each fit. The straight lines in Figure 4 indicate these predicted optical magnitudes and distances. Although all the information in Figure 4 is derived purely from the X-ray spectrum, a number of additional constraints can be brought to bear to further restrict the allowed range of parameters. First, the G″ optical counterpart has magnitudes $V = 25.2 \pm 0.3$ (Halpern & Tytler 1988) and $B = 26.5 \pm 0.5$ (Bignami, Caraveo, & Paul 1988). Since the $B - V$ color is redder than Rayleigh-Jeans, it would be unreasonable for the extrapolated X-ray spectrum to exceed the optical brightness. This would seem to rule out distances smaller than 150 pc in Figure 4.

Additional restrictions on the distance can be gleaned from the measured interstellar column densities in the direction of Geminga. These come principally from absorption-line studies of nearby stars; the derived column densities as a function of distance in the Galactic plane have been summarized by Paresce (1984) and Frisch & York (1983). The column density toward Geminga is small, but it is poorly determined because very few stars have been studied, and this direction grazes the edge of the local bubble which is devoid of neutral material to large distances in the third Galactic quadrant. What can be most reliably extracted from these surveys (in particular, from Figure 1 of Frisch & York and Figure 4 of Paresce) is that $N_{\rm H}$ does not rise to 1×10^{20} cm^{-2} until a distance of at least 150 pc is reached. It is also possible that a distance of ~ 500 pc is necessary for $N_{\rm H}$ to reach this value. So the allowed range of distances can conservatively be restricted to 150–450 pc by comparing the X-ray spectral fit in Figure 4 with these published measurements of the local interstellar column density.

A final restriction on the distance comes from the requirement that the apparent γ-ray luminosity not exceed the spindown power $I\Omega\dot{\Omega}$, or at least not greatly, since some beaming is possible. The implied upper limit is ~ 400 pc (Bertsch et al. 1992). So when all the constraints are combined, the best estimate of the distance to Geminga is 250 pc, with an allowed range of 150–400 pc. The corresponding range of X-ray spectral parameters in the restricted space of Figure 4 is $T_1 = (5.2 \pm 1.0) \times 10^5$ K, and $N_{\rm H} = (1.5 \pm 0.5) \times 10^{20}$ cm^{-2}.

Of the assumptions that could affect this distance estimate, one might at first suspect the "full surface" condition, since if the assumed area of the emitting surface is incorrect, the distances indicated in Figure 4 are changed. But in fact, the acceptable *range* of distances is insensitive to changes in the effective emitting area. Although the individual distance contours indicated in Figure 4 would change, the extrapolated optical magnitudes cannot. Neither would the fit $N_{\rm H}$, the observed interstellar column densities, nor the γ-ray efficiency limit. Similarly, the assumed form of the "hard" X-ray component does not significantly affect the fit to the soft component, so the distance limits indicated in Figure 7 are the same as those in Figure 4. The *combination* of conditions restricting the distance to between 150 and 400 pc is quite robust, and a much more accurate determination of the X-ray spectral parameters would have to be made before the uncertainty in distance could be reduced. A better determination of the actual run of column density versus distance in the direction toward Geminga would also be helpful in pinning down the distance. If the distance estimate presented here is flawed, it is more likely to be a result of gross errors in the detector response matrix, or substantial deviations of the spectrum from a blackbody as considered in §5.4, neither of which are obviously present.

5. INTERPRETATIONS

5.1. *Into the Valley of Death*

Similarities among the γ-ray spectra and most of the light curves of the known γ-ray pulsars (Crab, Vela, PSR 1706–44, Geminga) suggest that a similar, powerful accelerator is operating in each of their magnetospheres. If this is indeed the case, such an accelerator would have to be located in their outer magnetospheres ($r >> R \sim 10^6$ cm). This would almost certainly be

true for the source of the Crab pulsar's optical radiation. Synchrotron emission seems to be the only (incoherent) mechanism which is powerful enough to produce the Crab's optical light, and the radiating $e^{\pm}$ pairs must move relativistically to give the sharply peaked light curve. This limits the local magnetic field to $B \lesssim 10^8$ G, which is found only near the light cylinder, at $r_{lc} = c/\Omega \sim 10^8$ cm. But the arrival phase of each of the Crab's two optical pulses is identical to those of its X-rays and γ-rays. This strongly implies a common geometrical location for all of the radiation very far from the stellar surface.

Independent arguments for an outer-magnetosphere accelerator come from the *COS B* and *EGRET* observations of Geminga. First, γ-ray emission remains strong up to 5 GeV (Grenier, Hermsen, & Hote 1991). Such γ-rays would be converted to $e^{\pm}$ pairs if they crossed a $B \gtrsim 2 \times 10^8$ G, and thus would not be expected to escape if produced within much less than $10\,R$ of the stellar surface. In addition, the maximum potential drop along $\vec{B}$ which can be sustained within that distance to the star is about 10^{12} V. At higher voltages, curvature radiated γ-rays would produce so many $e^{\pm}$ pairs as they crossed the local $B > 10^9$ G, that such pair production would quench the accelerating potential drop. The maximum possible particle flow ($\dot{N}_0$) through any accelerator along the open field-line bundle between Geminga's surface polar cap and its light cylinder is limited to

$$\dot{N}_0 < \frac{\Omega^2 B_p R^3}{ec} \sim 8 \times 10^{31}\ \mathrm{s}^{-1}, \tag{3}$$

where B_p is the dipole field component at the stellar surface. (A current larger than $e\dot{N}_0$ would itself cause a local B near the light cylinder which is larger than that from the star.) Therefore, the maximum power from an inner magnetosphere accelerator is $e\dot{N}_0 \times 10^{12}\mathrm{V} \sim 10^{32}$ ergs s^{-1}. But Geminga's γ-ray flux in the 50–5000 MeV range is $\sim 3.1 \times 10^{-9}$ ergs cm $^{-2}$ s^{-1} (Grenier et al. 1991), corresponding to a luminosity of 2.3×10^{34} ergs s^{-1} if radiation is emitted isotropically at the estimated distance of 250 pc. Indeed, any magnetosphere accelerator which manages to mobilize a large fraction of a pulsar's total spindown power ($I\Omega\dot{\Omega} \sim 3.3 \times 10^{34}$ ergs s^{-1} for Geminga) must be very far from that pulsar's surface unless the pulsar is near its radio death line (Ruderman & Sutherland 1975; Chen & Ruderman 1993). The maximum possible potential drop between the surface and the light cylinder of Geminga is

$$\Delta V_{max} \sim \frac{\Omega^2 B_p R^3}{2c^2} \sim \frac{I\Omega\dot{\Omega}}{e\dot{N}_0} \sim 2 \times 10^{14}\ \mathrm{V}, \tag{4}$$

and almost all of it must be used to account for Geminga's very large apparent L_γ. Because the apparent L_γ is so close to the theoretical maximum ($\sim I\Omega\dot{\Omega}$), it is likely that there is a favorable beaming geometry which enhances the flux in our direction.

The "outer-gap" accelerator model was proposed to explain needed pair production and associated energetic photon emission in the outer magnetospheres of the Crab and Vela pulsars. Such models may have application to all of the γ-ray pulsars. A turn-off for strong γ-ray emission from a Vela-like pulsar was predicted at a period $P \sim 0.13$ s by Ruderman & Cheng (1988). This period depended upon the characteristic magnetic field through the accelerator which extends along the closed field-line boundary from the "null surface" where $\vec{\Omega} \cdot \vec{B} = 0$ out to the light cylinder. For an aligned pulsar, the outer end of the accelerator is at $r_{max} = r_{lc} = c/\Omega$. The inner end is at $r_{min} = (2/3)\, r_{lc}$, but it moves in sharply with increasing angle between the stellar dipole moment $\vec{\mu}$ and the spin $\vec{\Omega}$ until $r_{min} \sim (4/9)\,(\vec{\mu} \cdot \vec{\Omega})^2 \mid \vec{\mu} \times \vec{\Omega} \mid^{-2} r_{lc}$. The turn-off period $P \sim 0.13$ s comes from taking the characteristic B in the accelerator as that at r_{lc}. Chen and Ruderman (1993) used B evaluated at $r = 0.5\, r_{lc}$ which gives a γ-ray death line defined by $5 \log B_p - 12 \log P = 69.5$. Geminga, with $B_p = 1.6 \times 10^{12}$ G, falls just below this line, i.e., just beyond turn-off. However, because a substantial inclination angle between $\vec{\mu}$ and $\vec{\Omega}$ moves the inner end of the accelerator nearer to the star, it increases the accelerator's magnetic field. This

could account for Geminga being a strong γ-ray pulsar rather than a moribund one. Indeed, if Vela's inclination angle, $\theta = \cos^{-1}(\hat{\mu} \cdot \hat{\Omega})$, is $\sim 35°$, and if Geminga's is $\sim 65°$, then their "outer-gap" accelerators could have similar local magnetic field, size, current flow, and total power (Ruderman et al. 1993). Geminga's accelerator would, however, have to span almost all of that star's accessible open field lines to accomplish this, compared to less than 1/3 of the open field lines for Vela's. With this modified inclination angle, an outer-gap model which worked for Vela would probably also be applicable to Geminga. Reports of the death of such models (Bertsch et al. 1992) seem exaggerated, or at least premature.

5.2. *Beam Geometry*

Certain features of a Geminga-like outer magnetosphere accelerator seem robust enough to survive in any model of an accelerator and γ-ray emission in that region. To motivate these we shall, however, use the description of an outer-gap, Vela-like accelerator (Cheng et al. 1986a).

a) The accelerator, to avoid self-quenching by its own $e^{\pm}$ pair production, is bounded by the last closed field-line surface of Figure 8. There is a similar accelerator on either side of the star.

b) Electrons and positrons accelerated through the accelerator are radiation-reaction limited, so that each accelerator is almost 100% efficient as a γ-ray emitter.

c) To achieve the high $L_\gamma/I\Omega\dot{\Omega}$ of Geminga, almost all of the appropriately curved open field lines which pass through the $\vec{\Omega} \cdot \vec{B} = 0$ surface also pass through the outer-magnetosphere accelerator.

d) Because of $e^{\pm}$ pair production within the accelerators, each produces a particle flux $\dot{N}$ of $e^-(e^+)$ moving down toward the star's polar cap from its inner end, and an equal flux of $e^+(e^-)$ moving outward from its light cylinder. In addition, there is a comparable flux of positively (negatively) charged particles pulled up from the polar caps which also passes through the accelerator. The total (maximum) flux of $e^-(e^+)$ directed down toward the polar caps is

$$\dot{N} \sim 2 \left(\frac{\Omega B}{2\pi e}\right) \left(\frac{\pi}{2}\frac{R}{r_{lc}}\right) R^2 \sim 4 \times 10^{31}\ s^{-1}. \qquad (5)$$

These $e^-(e^+)$ will emit the curvature radiation beams 2 and 2′ of Figure 8.

e) Within the accelerator, pair-produced e^- and e^+ flow in both directions so that the similar fan beams of radiation, beams 1 and 1′ from one accelerator, will be matched by beams 3 and 3′ from the other. Because of Geminga's large tilt angle θ, the curvature radiation beam 2 will only be seen by observers looking within an angle θ of the pulsar spin axis. It is less clear over how large an angle the fan beams 1 and 3 would be observable.

f) An observer could, in principle, see the three beams 1, 2, and 3 (or 1′, 2′, and 3′). Because of Geminga's large tilt angle, the emission radius $r_e << r_{lc}$ and time-of-flight and aberration differences among the three beams are small. The phase separation between beams 1 and 2 is $\Delta\phi = 0.5 + \delta$ with $\delta \sim 2r_e/\pi r_{lc}$. Beams 1 and 3 will merge with separation δ. Geminga's observed $\Delta\phi$ and the widths of its two pulses require $r_e < 0.05\, r_{lc} = 5 \times 10^7$ cm. This would imply an inclination angle for Geminga greater than 70°.

g) Because of this large angle, beams 2 and 2′, and even 1′ and 3, may come close enough to the strong inner magnetic field of the star to give a very substantial $e^{\pm}$ pair production there.

5.3. *Polar-Cap Heating*

The extreme relativistic particles from the starward end of the accelerator will curvature radiate away much of their energy before reaching the stellar polar caps. Their instantaneous rate of such energy loss is

$$\dot{E} = \dot{\gamma} mc^2 = -\left(\frac{2c}{3}\right)\left(\frac{e}{r_c}\right)^2 \gamma^4, \qquad (6)$$

where $r_c \simeq (rc/\Omega)^{1/2}$ is the local radius of curvature of the (dipole) field lines which link the accelerator to the star's polar cap. For an accelerator which begins at the radius $r_{\rm min} >> R$, the residual energy of the $e^{\pm}$ impacting the polar cap can be approximated as

$$E(R) = \left[\frac{2e^2\,\Omega}{mc^3}\ln\left(\frac{r_{\rm min}}{R}\right)\right]^{-1/3} mc^2 \sim 6.5 \text{ ergs}, \tag{7}$$

as long as $E(r_{\rm min}) >> E(R)$. Then from equation (5), and choosing $r_{\rm min} \sim r_e \sim 5 \times 10^7$ cm, the power brought down to the polar cap by particles coming from the inner ends of the outer-magnetosphere accelerator is $L_p \sim 2.6 \times 10^{32}$ ergs s^{-1}. This predicted polar-cap luminosity is insensitive to the geometry, location, or pair-production mechanisms in the accelerator, but it does assume that the accelerator current (and power) are near maximal.

If the two heated half polar caps could be directly observed, they would have a temperature of $\sim 6 \times 10^6$ K. This is about twice the observed temperature $T_2 = (3 \pm 1) \times 10^6$ K of the hotter blackbody component. Moreover, the theoretical polar-cap heating exceeds the "hard" X-ray luminosity by a factor of 10^2, and is even a few times larger than the estimated total X-ray emission (see Table 4). While relatively small changes in Geminga's parameters (e.g., increasing the distance by a factor of 2) could accommodate an X-ray luminosity of $\sim 2 \times 10^{32}$, how the polar cap radiation is degraded in temperature by a factor of 10 remains a problem. Moreover, the observed X-rays seem to be radiated at 5×10^5 K from almost the entire neutron star surface area of 10^{13} cm^2, instead of from the 10^9 cm^2 polar cap.

One possible cause for this discrepancy arises in the large density of $e^{\pm}$ pairs near the neutron star. Their effectiveness in reflecting keV X-rays from a hot polar cap is enormously increased whenever their cyclotron resonance frequency in the strong local magnetic field matches the frequency of incident X-rays. We consider next some aspects of this problem.

5.4. *Circumstellar X-ray Scattering*

In the geometry of Figures 8 and 9, the radiation beams 2 and 2′ can pass relatively close to the neutron star before leaving the magnetosphere. (This may also be true for beams 3 and 1′.) A 10 GeV γ-ray would be converted into an $e^{\pm}$ pair by Geminga's magnetic field if it came within 3×10^7 cm of the star; a 100 MeV γ-ray would convert if it approached within 6×10^6 cm $\simeq 6R$. The $e^{\pm}$ pairs materialized from the γ-rays of energy E_γ would themselves radiate γ-rays with energy $E_\gamma^{(2)} \sim 10(E_\gamma/\text{GeV})$ MeV. This second generation of γ-rays could in turn also make pairs if some passed within a radius $r \sim R(E_\gamma^{(2)}/\text{MeV})^{1/3}$ of the star. The pair flux thus generated increases with larger inclination angles between $\vec{\mu}$ and $\vec{\Omega}$, and might exceed 10^{38} s^{-1} for Geminga. These $e^{\pm}$ pairs are created mainly on closed field lines and will, therefore, ultimately be channeled into the near magnetosphere of the neutron star. Their abundance there depends upon the detailed location of the annihilation process, e.g., to what extent polar-cap X-ray emission and cyclotron resonant $e^{\pm}$ scattering of those X-rays keeps these pairs from flowing easily down onto the stellar surface. Local number densities $n_\pm > 10^{15}$ cm^{-3} and column densities in excess of 10^{21} cm^{-2} seem quite plausible for Geminga.

With only a Thomson scattering cross section σ_T, these $e^{\pm}$ would have a negligible optical depth to escaping polar-cap X-rays. However, because of the stellar magnetic field the effective X-ray $e^{\pm}$ scattering cross section can be represented as

$$\sigma = \sigma_T(\hat{\mathcal{E}}\cdot\hat{B})^2 + \frac{2\pi^2e^2}{mc}\,|\,\hat{\mathcal{E}}\times\hat{B}\,|^2\;\delta(\omega_B - \omega). \tag{8}$$

Here $\hat{\mathcal{E}}$ is the (electric field) polarization of the X-ray, and $\omega_B = eB(r)/mc$. With $\hbar\omega \simeq 0.5$ keV for Geminga's polar-cap X-rays, and $\hat{\mathcal{E}}\cdot\hat{B} = 0$,

$$\int_R^\infty \sigma\,dr = \frac{2\pi^2}{3}\left(\frac{e^2R}{mc\,\omega}\right)\left(\frac{eB_p}{mc\,\omega}\right)^{1/3} \sim 2 \times 10^{-13}\text{ cm}^3. \tag{9}$$

Thus an $n_{\pm} > 10^{13}$ cm^{-3} at $r \sim 3\,R$ would make an optically thick cyclotron resonant backscattering layer there. Most of the hot polar cap X-rays would then not escape before being intercepted by the star. In this way, polar cap X-ray power is transferred to the entire stellar surface from which it is reradiated at a predicted lower temperature T_1, where

$$T_1 \sim \left(\frac{\text{polar cap area}}{4\pi\, R^2}\right)^{1/4} T_2 = \left(\frac{\Omega R}{4c}\right) T_2 = 0.12\, T_2. \tag{10}$$

The predicted ratio T_1/T_2 is in reasonable agreement with the observed values and their errors as listed in Table 2. Of course, the cooler surface radiation will have to pass through its own cyclotron resonant $e^{\pm}$ backscattering layer at $r \sim 6\,R$ before ultimately escaping. However, there is no significant further reduction in emitted X-ray energy even if some of this softer X-ray flux is also ultimately reabsorbed by the stellar surface, although the spectral shape of the emission can be affected.

A small fraction of the hard polar cap X-rays may pass through the resonant scattering layer at $r \sim 3\,R$ without being backscattered. These are the photons with $|\,\hat{\mathcal{E}} \times \hat{B}\,| \sim 0$. They are moving almost perpendicular to the local $\vec{B}$ with polarization along $\vec{B}$, so that any cyclotron resonances are not effective in amplifying their cross section. Thus, the hard X-ray component which passes through the cyclotron resonance backscattering layer might be almost completely linearly polarized.

5.5. *X-ray Light Curves*

Any model which tries to explain as other than a coincidence the 180° separation of Geminga's two γ-ray peaks would need a highly inclined dipole. Then, if the stellar surface magnetic field configuration were nearly that of the canonical central dipole (two surface polar caps 180° apart), the hard $\sim$ 1 keV polar cap radiation would be expected to show two similar peaks separated by 0.5 in phase. Rather, the data comprise a single peak, or perhaps two peaks sufficiently close together in phase to be unresolvable in data of the present quality. This suggests a sunspot-like configuration, such as that from a dipole much nearer the surface than a centrally located one. Radiation from a sunspot polar-cap configuration should appear brightest to an observer when the star is rotated by about 90° from the phase angle at which γ-ray beam 2 is observed (Figure 9a). With the highly inclined dipole and sunspot-like geometry of Figure 9b, this emission direction is also near that for which some of the beam can have $|\,\hat{\mathcal{E}} \times \hat{B}\,| \sim 0$ (i.e., $\vec{B}$ perpendicular to the direction of propagation of the photon), and thus pass through the circumstellar $e^{\pm}$ cyclotron resonant scattering layer instead of being scattered back toward the star. The maximum hard X-ray intensity would then be expected at a phase interval $\Delta\phi \sim 0.25$ before or after γ-ray beam 2, depending on the sense of the stellar spin.

The most difficult place for the stellar X-rays to pass through the circumstellar $e^{\pm}$ resonance layer at $3R \lesssim r \lesssim 6R$ are the areas near the two open field-line bundles, because there $\vec{B}$ and $\vec{r}$ are nearly parallel. Any X-ray photon moving nearly radially outward there would have $|\,\hat{\mathcal{E}} \times \hat{B}\,| \sim 1$ so that the dominant resonant part of the scattering cross section in equation (8) is a maximum. This would cause a minimum in the observed X-ray intensity approximately coincident in phase with the γ-rays of beam 2 since these come to us from this same open field-line bundle direction. The indicated phases of the total X-ray minimum, hard X-ray maximum, and γ-ray beam 2 are sketched in Figure 10.

There is not yet a compelling determination of which of the two observed γ-ray beams should be identified with beam 2. However, beam 2 of Figure 8 should consist mainly of curvature radiation from $e^-(e^+)$ after they have left the accelerator. It would be expected to be less intense than the sum of beam 1, which contains similar radiation from $e^+(e^-)$ moving outward within and above the accelerator, plus beam 3 from inward moving $e^-(e^+)$ within and above the accelerator on the opposite side of the neutron star. This suggests identifying the weaker of Geminga's two γ-ray pulses (in Figure 10) as beam 2. More compelling support would be a softer spectrum at the highest energies for the weaker pulse, as its most energetic

γ-rays are converted to $e^{\pm}$ pairs when passing through the stellar magnetic field. If the second, stronger γ-ray pulse is mainly beam 3 of Figure 8, then its preceeding interpulse shoulder is also suggestive of what is expected from the effects of aberration on emission at larger radii (Cheng et al. 1986b). The model phases for Geminga's X-ray maxima and minima shown in Figure 10 are qualitatively similar to the observed ones in Figure 2.

[A comparison of the expected polar-cap heating with the observed X-ray luminosity can also be made for the Vela pulsar. Here the Ω and B are larger, but the fraction of open field lines subtended by the accelerator is probably of order 10% so that the expected polar-cap heating is $\sim 4 \times 10^{32}$ ergs s^{-1}, about the same as for Geminga. The observed X-ray luminosity in the Vela point source is 4.3×10^{32} ergs s^{-1} (Ögelman et al. 1992), which is in excellent agreement with such a model, but the inferred emitting area of 0.1 times $4\pi R^2$ is more difficult to understand: though it is much larger than the polar cap, it is still much smaller than the full surface.]

5.6. *Neutron Star Cooling Curves*

In the above interpretation, the soft X-ray component of luminosity $\sim 5.4 \times 10^{31}$ ergs s^{-1} comes from the stellar surface. Since the observed temperature of 5×10^5 K falls on the theoretical neutron star cooling curves, there may be no necessary reason to attribute the soft X-ray luminosity exclusively (or even mainly) to polar-cap heating. In view of the highly efficient conversion of the 3×10^{34} ergs s^{-1} spindown power to radiation, it is remarkable that the soft X-rays from Geminga still fall within the range allowed by the cooling curves. The predictions of a variety of models as presented by Page & Applegate (1992) fall in the range $(1-7) \times 10^5$ K for a neutron star of age 3×10^5 yr, and the Geminga data do not strongly discriminate among these. However, Page (1993) concludes that Geminga must have a superfluid core in order for its surface temperature to be compatible with most cooling scenarios. Given the expectations for polar-cap heating, and the fact that the soft X-ray luminosity is only $\sim 10^{-3}$ of the spindown power, the observed temperature $T_1 = (5.2 \pm 1.0) \times 10^5$ K must be regarded as only an upper limit when comparing with theoretical cooling curves. An additional reason to interpret T_1 as an upper limit is the effect of the surface magnetic field on the emergent spectrum, as discussed in the next section.

The shape of Geminga's soft X-ray pulse is very similar to that of PSR 0656+14 (Finley et al. 1992) although the statistics of the latter are poorer because the pulsed fraction is only 14%. The blackbody temperature of PSR 0656+14 is 9×10^5 K, and its characteristic age is 1.1×10^5 yr, a factor of 3 younger than Geminga. There is so far no evidence for γ-ray emission from PSR 0656+14 ($d \sim 500$ pc), nor for an additional hard X-ray component. These facts together are consistent with the interpretation of the soft X-ray spectrum in both of these stars as "normal" photospheric emission.

5.7. *Magnetized Neutron Star Atmospheres*

The X-ray spectrum emergent from a realistic neutron star atmosphere can deviate substantially from a blackbody because of the non-grey opacity (Romani 1987). The observed spectrum is generally harder than a blackbody at the given effective temperature. The surface magnetic field ameliorates this effect to some extent, but also introduces rotational modulation because the radiative opacity and heat conduction are anisotropic (Miller 1992; Shibanov et al. 1992a,b; Ventura et al. 1992). These authors have modelled both fully ionized and partially ionized atmospheres, and the deviations are more substantial for the latter with light element composition, since the K-edges of hydrogen and helium are shifted into the *ROSAT* bandpass for typical surface magnetic fields. Although a detailed fitting of these models is beyond the scope of this paper, a first-order concern is whether or not magnetic effects can account for the complex spectral and pulse behavior in terms of a *single* component spectrum, without the need for two distinct blackbodies as invoked in § 3. The light-element models are the most relevant in this regard.

Beginning with a fully ionized hydrogen photosphere, Shibanov et al. (1992a) showed that two models with effective temperature 5×10^5 K and $B = 4.7 \times 10^{12}$ G can differ by as

much as 45% in flux at 1 keV, according to whether the magnetic field is normal or tangential to the surface. At lower energies the difference is less, and below 0.25 keV the spectra cross over. Although this anisotropy could in principle be responsible for some of the rotational modulation, it seems unlikely to be able to explain the *existence* of the hard pulse as a tail of the soft blackbody, since the observed flux at 1 keV is at least 100 times larger than the extrapolation of the soft blackbody component (Figure 3).

The inclusion of bound-free opacity causes sharper deviations from a blackbody (Miller 1992; Shibanov et al. 1992b). The theoretical spectrum closely follows a blackbody below the photoionization threshold of hydrogen, which is at ~ 200 eV for $B \sim 2 \times 10^{12}$ G. Deviations can be substantial above this energy. In particular, the spectra fall below the blackbody between 0.2 and 0.6 keV, but rise to as high as 10 times the blackbody flux at 1 keV. Miller (1992) presented only models for $T = 1 \times 10^6$ K, but it is likely that the deviations would be even larger at lower temperatures. It is not clear whether the observed X-ray spectrum and pulse behavior can be explained by these models, and it appears that only the hydrogen atmosphere is a candidate since all the heavier element atmospheres produce large flux deficits around 1 keV (Miller 1992). Although a two-component model may remain a necessity, it would nevertheless be very be useful to investigate the effects of more realistic model atmospheres on the parameters derived from the soft X-ray spectrum.

5.8. *Absence of Radio Emission*

Geminga has not been detected as a radio source. Models for its 180° double-pulsed γ-ray emission suggest that it has a much more inclined dipole than most canonical radio pulsars, together with a favorably inclined line of sight to the observer. With such a geometry, it is difficult to see why Geminga's radio beams should be missed by observers who can see its γ-rays. A *radio-quiet* Geminga may, on the other hand, be just what is expected for such a neutron star. Radio emission is generally thought to be powered by an inner-magnetosphere accelerator, perhaps even one which forms just above the polar caps where the star cannot supply the Goldreich-Julian charge density, $\rho = \vec{\Omega} \cdot \vec{B}/2\pi c$, needed to maintain $\vec{E} \cdot \hat{B} = 0$. Near Geminga's surface, this requires a charge density $n \sim 5 \times 10^{11}$ cm^{-3} and a possible flux $cn \sim 1.4 \times 10^{22}$ cm^{-2} s^{-1}. If much more charge and $e^{\pm}$ flow than this is introduced into the accelerator region, they will quench that accelerator's $\vec{E} \cdot \hat{B}$ and, presumably, the radio emission which it supports.

Geminga appears to be an exceptionally good candidate for a pulsar in which γ-ray emission from an outer-magnetosphere accelerator produces enough $e^{\pm}$ pairs in the inner magnetosphere to quench a radio-emission accelerator which would otherwise form there. This could be accomplished by the $e^{\pm}$ pair production discussed in § 5.4. Intense γ-ray beams, e.g. beams 2 and 2′ of Figure 9, also make pairs on the upward curving open field lines on which inner-magnetosphere accelerators are expected. A large fraction of these pairs flow in toward the star and through any near polar-cap accelerator. That accelerator would be quenched if the inward flowing $e^{\pm}$ production rate is $\dot{N}_{\pm} \gtrsim 4\pi R^2 \, cn(R) \sim 2 \times 10^{35}$ s^{-1}. A rate exceeding this is quite plausible for Geminga because of the large intensity of its inward directed γ-ray beams (e.g., beams 2 and 2′ of Figure 9). For this radio-suppressing mechanism to be effective, both a high efficiency for converting spindown power into γ-rays, and a large inclination so that a significant fraction of these γ-rays pass close enough to the star to be converted into $e^{\pm}$ pairs, are needed.

6. UNIDENTIFIED GALACTIC γ-RAY SOURCES

Two recent developments in our understanding of the population of high-energy γ-ray sources motivate a reevaluation of the likelihood that isolated pulsars can account for the majority of the still unidentified *COS B* sources in the Galactic plane. The first is the discovery that Geminga and PSR 1706–44 (Thompson et al. 1992), which are older and spin less rapidly than than the Vela pulsar, also have higher γ-ray efficiencies. The efficiency of PSR 1706–44 is 7% assuming isotropic emission, and it was argued here that Geminga's efficiency is close to unity. The second development is the reanalysis of the *COS B* catalog by Mayer-Hasselwander

& Simpson (1990) with a better diffuse background model, which leaves fewer still unidentified strong sources and a larger scale height for them. These trends tend to expand the pool of potential γ-ray sources, and to decrease the distance and hence the luminosity at which they are detected.

The number of "confirmed" *COS B* sources above a threshold of approximately 3×10^{-10} ergs cm^{-2} s^{-1} is only eight. The average height above the Galactic plane for these is 2.°7, which is roughly twice that of the 24 sources in the 2CG catalog (Swanenburg et al. 1981). Many of the former "sources" closest to the plane were in reality enhancements in the diffuse flux. But ten new sources were suggested by the reanalysis. These have lower fluxes, and an even larger scale height of $\sim 6°$. Presumably the better background model enables fainter sources to be found only slightly away from the plane, so that their latitude distribution probably overestimates the true scale height of the Galactic γ-ray source population. If a population of young pulsars is to account for the *COS B* sources, they should have a scale height of ~ 80 pc, reflecting the location of their birth in a young stellar population. Adopting a scale height of 3° implies a typical distance of 1.5 kpc, rather than the 2–7 kpc originally assumed by Swanenburg et al. (1981).

The number of potential sources with flux greater than $F_{\rm min} \sim 3 \times 10^{-10}$ ergs cm^{-2} s^{-1} can be estimated from the birth rate of pulsars in the solar neighborhood, $\sim 2.2 \times 10^{-5}$ yr^{-1} kpc^{-2} (Lyne & Smith 1990). If the apparent γ-ray luminosity is a fraction η of the spindown power, then $L_\gamma = 4 \times 10^{31} \eta B_{12}^2 P^{-4}$ ergs s^{-1}, where B_{12} is the surface field in units of 10^{12} G. (Any increase in apparent luminosity due to beaming is considered here to be included in η.) The characteristic age of a pulsar is $\tau = 1.6 \times 10^7 P^2 B_{12}^{-2}$ yr, so the maximum distance to which a pulsar of age τ could be detected is $r_{\rm max} = (L_\gamma / 4\pi F_{\rm min})^{1/2} = 5.3\, \eta^{1/2} (B_{12} \tau_5)^{-1}$ kpc, where τ_5 is the age in units of 10^5 yr. The efficiency η is very likely a function of age, as indicated by the trend among the four known γ-ray pulsars. A typical value for η of 0.1 will first be examined, and then a parameterization of the form $\eta = 0.2\, \tau_5$ will be used.

Since pulsars younger than age τ_5 would be detectable at the distance $r_{\rm max}$, the surface density of *detectable* pulsars at a distance r is $\sigma(r) = 2.2\, \tau_5\, \beta = 11.6\, \eta^{1/2}\, \beta (B_{12} r)^{-1}$ kpc^{-2}, where β is the fraction of γ-ray pulsars whose beaming allows detection by us. For the case of constant η, the total number of detectable pulsars to a distance D is then

$$N = \int_0^D 2\pi\, r\, dr\, \sigma(r) = 73\, \frac{\eta^{1/2} \beta}{B_{12}}\, D, \tag{11}$$

where D is in kpc. A typical value of D can be the distance at which the flux of a Vela-like pulsar would equal $F_{\rm min}$, or ~ 3 kpc. For $\eta \beta^2 \sim 0.1$ and $B_{12} \sim 3$, we find $N \sim 23$, which can account for the *COS B* sources.

For a model in which $\eta = 0.2\, \tau_5$, the maximum distance to which a pulsar is detected can be written as $r_{\rm max} = 2.4\, B_{12}^{-1}\, \tau_5^{-1/2}$ kpc, and the surface density of detectable pulsars at a distance r is $\sigma(r) = 12\, (B_{12} r)^{-2} \beta$ kpc^{-2}. The total number of detectable pulsars is then

$$N = \int_{D_{\rm min}}^{D_{\rm max}} 2\pi\, r\, dr\, \sigma(r) = \frac{76\, \beta}{B_{12}^2} \ln \left(\frac{D_{\rm max}}{D_{\rm min}} \right) \tag{12}$$

Choosing $B_{12} \sim 3$, $\beta = 1$, and $D_{\rm max}/D_{\rm min} \sim 15$ to represent the expected range of distance between the nearest source (Geminga) and the furthest, we find $N \sim 23$ as before.

These rough calculations show that if γ-ray efficiencies of pulsars in the period range $0.1 - 0.24$ s are typical of the ones so far detected, then the standard pulsar birth rate can account for the γ-ray source population. This birth rate assumes a beaming factor of 5 for the *radio* emission. The estimates for η used in the calculation of the detectability of the γ-rays do not assume any correlation between radio and γ-ray beaming patterns, and thus do not require the *COS B* sources to be known radio pulsars. But should we worry that the detected γ-ray pulsars might have exceptionally high γ-ray efficiencies that are *atypical* of their contemporaries?

Although this is a concern, there seems to be no strong evidence that it is the case. Pulsars of the age of PSR 1706–44 or younger (17,000 yr) should be distributed with a mean separation of 1.6 kpc. Its actual distance from us of 1.4 kpc is in line with this expectation. Similarly, pulsars which are younger than Geminga (340,000 yr) have a mean separation of $\sim$ 370 pc. The estimated distance to Geminga of 250 pc is, therefore, also typical. Vela itself, at a distance of 500 pc, is closer by a factor of 4 than the mean separation of 11,000 year old pulsars. So the evidence is that the detected γ-ray pulsars are *not* overachievers, but are rather typical representatives of their age groups.

7. COMMENTS

The *ROSAT* X-ray observation of Geminga can be interpreted in terms of thermal emission from the surface of the neutron star. A combination of constraints based on fits to the X-ray spectrum, the brightness of the optical counterpart, and the local interstellar hydrogen column can be used to restrict the likely distance to the range 150–400 pc. The surface temperature is $T_1 = (5.2 \pm 1.0) \times 10^5$ K, which is in the range of model cooling curves for a neutron star of age 3×10^5 yr. The bolometric soft X-ray luminosity is $5.4 \times 10^{31} (d/250\,\mathrm{pc})^2$ ergs s^{-1}, but could be in error by a factor of 2 because of the effect of the uncertainty in N_{H} on the X-ray spectral fits.

The implied efficiency for converting spindown power into γ-ray luminosity is then greater than 25%, and a substantial beaming factor could be required as well if the upper range of the distance estimate applies. Rather than all γ-ray pulsars having efficiencies comparable to Vela ($\eta \sim 1.4\%$), the observations of both PSR 1706–44 ($\eta \sim 7\%$) and Geminga strongly suggest that the efficiency is a rapidly increasing function of period. The effect of this trend is to boost the likelihood that most of the high-energy γ-ray sources in the Galaxy are pulsars with periods in the range 0.1–0.24 s. They are not necessarily known radio pulsars, both because γ-ray fan beams can be more widely visible than narrow radio beams, and because efficient inclined γ-ray pulsars may quench their radio emission accelerators (§ 5.8).

A highly inclined rotator is favored in order to account for the large γ-ray efficiency and the 180° separation of the γ-ray pulses. Since the γ-ray efficiency of Geminga is close to unity, it is of particular interest to ask how much additional luminosity might be hidden in in the energy band between the 1 keV X-rays and the 100 MeV γ-rays. A power law connecting the detections at these energies would contain only $\sim$ 24% of the *COS B* luminosity, and would fall below the detection thresholds of all existing instruments. The claimed 2.8 σ detection of pulsed emission from Geminga by the Figaro experiment (Massaro et al. 1993) lies above this interpolation, and amounts to a flux of 1.1×10^{-10} ergs cm^{-2} s^{-1} in the 0.15–0.48 MeV range. This is only 4% of the *COS B* flux, but, if real, it could be indicative of an energetically significant component if it extrapolates over a wider energy band. It could also contain more than 10^{38} s^{-1} of $e^{\pm}$ annihilation γ-rays which may come from the pair creation mechanisms of § 5.4.

Geminga is of great importance to the study of neutron star photospheres, since it presents the most detailed pulse profile and spectrum so far obtained that can be confidently attributed to surface emission. But the X-ray pulse shapes may be difficult to analyze quantitatively. The single-peaked nature of the soft and hard X-ray pulses and their $\sim$ 105° separation suggests a *surface* magnetic field geometry which includes an off-center dipole. It is not clear how much of the high-frequency structure in the soft X-ray pulse can be understood as rotational modulation of surface field, and to what extent resonant scattering in the magnetosphere may be responsible. The interpretation of the hard X-ray component ($T_2 \sim 3 \times 10^6$ K) as polar cap emission may yet be problematic: its luminosity of 2×10^{30} ergs s^{-1} falls two orders of magnitude below the expected polar-cap heating from the magnetospheric accelerator. Models in which the polar-cap emission can be redistributed over the surface, as in § 5.4, seem to deserve detailed investigation. High-resolution spectroscopy and better signal-to-noise ratio in the harder X-rays would be a blessing (or a curse) on efforts to understand the effects of the

surface magnetic field and any scattering processes on the emergent X-ray spectrum and pulse profile.

We thank Hakki Ögelman for his extensive and expert assistance with the absolute timing of the ROSAT data. This research was supported by NASA grants NAG 5-1606, NAG 5-2051, and NAG 5-2016. This paper is contribution 512 of the Columbia Astrophysics Laboratory.

TABLE 1
GEMINGA PULSE EPHEMERIS

Parameter	Value
T_0 (JD)[a]	2448329.886823149
P (s)	0.2370973861
$\dot{P}$ (s s^{-1})	1.0977×10^{-14}

[a] TDB time of phase 0 in Figures 1 and 2.

TABLE 2
FIT TO DOUBLE BLACKBODY MODEL

Parameter	Value	Confidence
T_1	5.2 (+1.0,–1.3) $\times 10^5$ K	68%
	(+1.2,–2.2)	90%
T_2	3.0 (+0.7,–0.6) $\times 10^6$ K	68%
	(+0.9,–0.7)	90%
$N_{\rm H}$	1.5 (+0.8,–0.5) $\times 10^{20}$ cm^{-2}	68%
	(+1.7,–0.6)	90%
f	3.5 (+4.5,–2.9) $\times 10^{-5}$	68%
	(+6.6,–3.4)	90%
C	162.	
F_1^a	7.2×10^{-12} ergs cm^{-2} s^{-1}	
F_2^a	2.6×10^{-13} ergs cm^{-2} s^{-1}	

[a] Bolometric flux in component before interstellar absorption.

TABLE 3
FIT TO BLACKBODY PLUS POWER-LAW MODEL

Parameter	Value	Confidence
T_1	4.5 (+1.4,–1.5) $\times 10^5$ K	68%
	(+1.6,–2.1)	90%
α	1.47 (+0.28,–0.37)	68%
	(+0.38,–0.55)	90%
N_H	1.85 (+1.3,–0.7) $\times 10^{20}$ cm^{-2}	68%
	(+2.4,–0.8)	90%
f	1.93 (+9.1,–1.9) $\times 10^{-7}$	68%
	(+12.1,–1.9)	90%
C	545.	
F_1^a	1.1 $\times 10^{-11}$ ergs cm^{-2} s^{-1}	

[a] Bolometric flux in blackbody component, before interstellar absorption.

TABLE 4
SUMMARY OF ENERGY BUDGET

Component	Luminosity (ergs s^{-1})
Spindown Power	3.3×10^{34}
γ-rays[a]	2.3×10^{34}
"Soft" X-rays[a]	5.4×10^{31}
"Hard" X-rays[a]	1.9×10^{30}

[a] Luminosity for a distance of 250 pc, in the isotropic case.

REFERENCES

Bertsch, D. L., et al. 1992, Nature, 357, 306
Bignami, G. F., Caraveo, P. A., & Mereghetti, S. 1992, IAU Circ. No. 5651
Bignami, G. F., Caraveo, P. A., & Paul, J. A. 1988, A&A, 202, L1
Brinkmann, W., & Ögelman, H. 1987, A&A, 182, 71
Chen, K., & Ruderman, M. 1993, ApJ, 402, 264
Cheng, K. S., & Helfand, D. J. 1983, ApJ, 271, 271
Cheng, K. S., Ho, C., & Ruderman, M. 1986a, ApJ, 300, 522
Cheng, K. S., Ho, C., & Ruderman, M. 1986b, ApJ, 300, 500
Finley, J. P., Ögelman, H., & Kiziloğlu, Ü 1992, ApJ, 394, L21
Frisch, P. C., & York, D. G. 1983, ApJ, 271, L59
Grenier, I. A., Hermsen, W., & Hote, C. 1991, Adv. Space Res., 11, (8)107
Halpern, J. P., & Holt, S. S. 1992, Nature, 357, 222
Halpern, J. P., & Tytler, D. 1988, ApJ, 330, 201
Hermsen, W., et al. 1992, IAU Circ. No. 5541
Lyne, A. G., & Smith, F. G. 1990, Pulsar Astronomy (Cambridge: Cambridge Univ. Press), 108
Massaro, E., et al. 1993, in Proc. Third Compton Observatory Science Workshop, in press
Mattox, J. R., et al. 1992, IAU Circ. No. 5583
Mayer-Hasselwander, H. A., et al. 1992, IAU Circ. No. 5649
Mayer-Hasselwander, H. A., & Simpson G. 1990, Adv. Space Res., 10, (2)89
Miller, M. C. 1992, MNRAS, 255, 129
Morrison, R., & McCammon, D. 1983, ApJ, 256, 92
Ögelman, H., Finley, J. P., & Zimmermann, H. U. 1992, Nature, in press
Page, D. 1993, in Proc. First Symp. on Nuclear Physics in the Universe, ed. M. R. Strayer & M. W. Guidry (Bristol: Adam Hilger & Co.)
Page, D. & Applegate, J. H. 1992, ApJ, 394, L17
Paresce, F. 1984, AJ, 87, 1022
Romani, R. W. 1987, ApJ, 313, 718
Ruderman, M., Chen, K., Cheng, K. S., & Halpern, J. P. 1993, in Proc. Third Compton Observatory Science Workshop, in press
Ruderman, M., & Cheng, K. S. 1988, ApJ, 335, 306
Ruderman, M., & Sutherland, P. G. 1975, ApJ, 196, 57.
Shibanov, Yu. A., Zavlin, V. E., Pavlov, G. G., & Ventura, J. 1992a, A&A, 266, 313
Shibanov, Yu. A., Zavlin, V. E., Pavlov, G. G., Ventura, J., & Potekhin, A. Yu. 1992b, in The Physics of Isolated Pulsars, Proc. Los Alamos Workshop on Isolated Pulsars, ed. K. A. Van Riper, R. I. Epstein, & C. Ho (Cambridge: Cambridge Univ. Press)
Swanenburg, B. N., et al. 1981, ApJ, 242, L69
Thompson, D. J., et al. 1992, Nature, 359, 615
Ventura, J., Shibanov, Yu. A., Zavlin, V. E., & Pavlov, G. G. 1992b, in The Physics of Isolated Pulsars, Proc. Los Alamos Workshop on Isolated Pulsars, ed. K. A. Van Riper, R. I. Epstein, & C. Ho (Cambridge: Cambridge Univ. Press)

FIGURE CAPTIONS

FIG. 1.– X-ray pulse profile folded according to the ephemeris of Table 1. The top panel shows all the data in the 0.07–1.5 keV range, and the lower three panels show the same data separated into three energy bands. The data are repeated for two cycles to guide the eye. Phase 0.0 corresponds to T_0 from Table 1.

FIG. 2.– A comparison of the X-ray and γ-ray pulses in absolute phase. Phase 0.0 corresponds to T_0 from Table 1. The γ-ray light curve is taken from Bertsch et al. (1992).

FIG. 3.– Fit of the double blackbody model to the X-ray spectrum of Geminga. (a) Raw counts and model spectra folded through the detector response matrix. (b) Unfolded spectral model.

FIG. 4.– Confidence contours for the parameters of the soft X-ray component in the double blackbody fit. The confidence levels correspond to the case of three interesting parameters ($T_1, N_{\rm H}$, and C). Visual magnitudes are extrapolated from the Rayleigh-Jeans tail of the blackbody fit, while distances assume emission from the full surface of a neutron star of radius $R = 10$ km.

FIG. 5.– Confidence contours for the parameters of the hard X-ray component in the double blackbody fit. The confidence levels correspond to the case of two interesting parameters (T_2 and f). Corresponding values of T_1 are given as dashed lines.

FIG. 6.– Fit of the blackbody plus power-law model to the X-ray spectrum of Geminga. (a) Raw counts and model spectra folded through the detector response matrix. (b) Unfolded spectral model.

FIG. 7.– Confidence contours for the parameters of the soft X-ray component in the blackbody plus power-law fit. The confidence levels correspond to the case of three interesting parameters ($T_1, N_{\rm H}$, and C). Visual magnitudes are extrapolated from the Rayleigh-Jeans tail of the blackbody fit, while distances assume emission from the full surface of a neutron star of radius $R = 10$ km.

FIG. 8.– Proposed geometry of the outer magnetosphere of Geminga, showing the accelerators and γ-ray beams powered by them. The accelerator, which is relatively empty of charge, is the stippled region. The accelerator on the right (left) is bounded from below (above) by the last closed field-line surface. The open field-line bundle between the accelerator and the polar cap (vertically shaded region) contains $\dot{N}$, the $e^-(e^+)$ flow out of the accelerator down toward the polar cap (see also Figure 9).

FIG. 9.– (a) Geometry of the surface magnetic field, showing the highly inclined sunspot dipole, and γ-ray and particle beams inwardly directed along the open field-line bundle. (b) Top view of the neutron star, showing the near-surface field configuration and the rotation phase for which an observer at the bottom of the figure would see the maximum hard X-ray flux. The dashed lines are the radial directions in which $| \hat{\mathcal{E}} \times \hat{B} |$ can vanish at $r \sim 3\,R$.

FIG. 10.– Schematic phase diagram of the γ-ray and X-ray light curves according to the theory presented in §§ 5.1–5.5. Qualitative similarities with the observational data shown in Figure 2 are apparent.

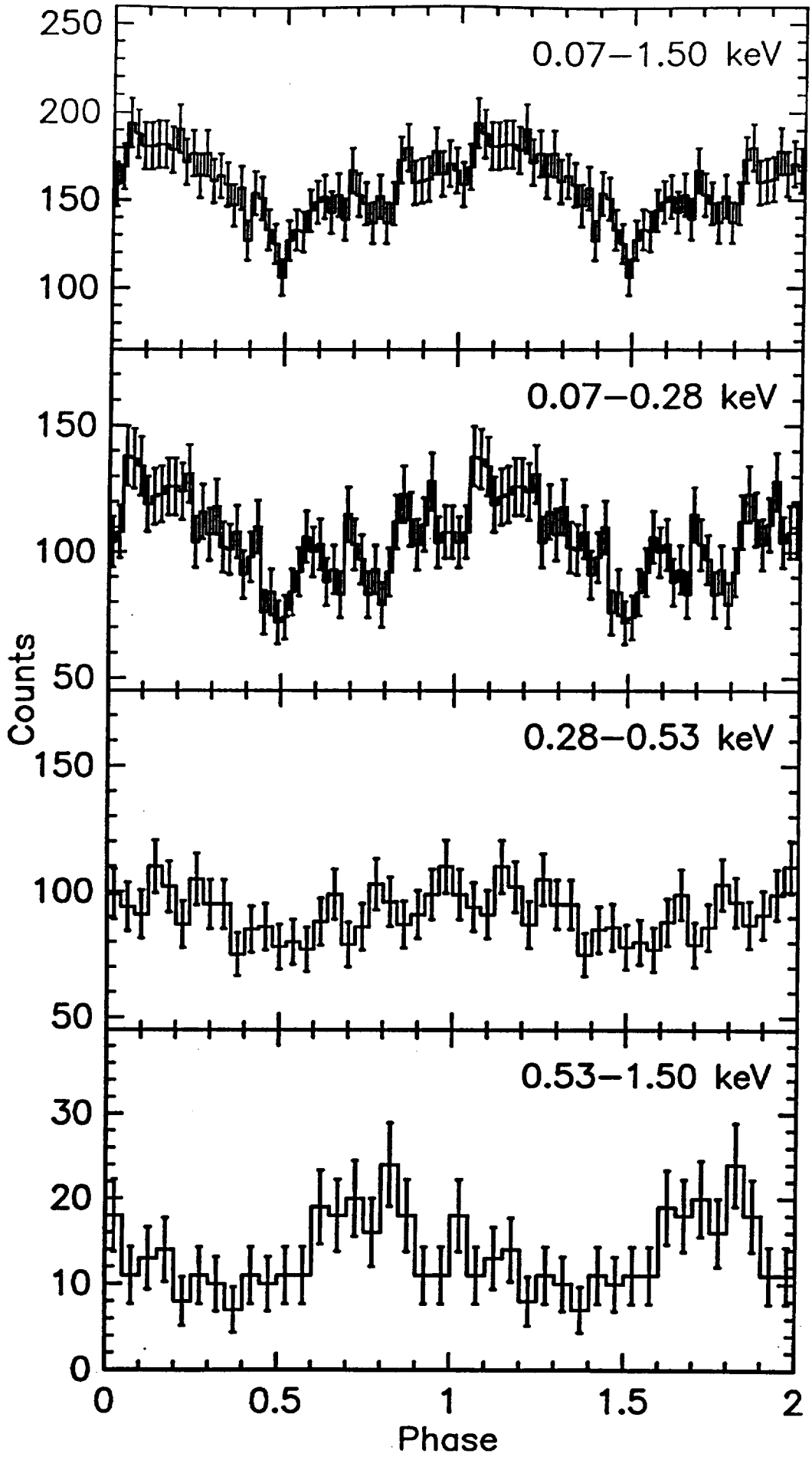
0.07–1.50 keV
0.07–0.28 keV
0.28–0.53 keV
0.53–1.50 keV
Counts
Phase
250
200
150
100
150
100
50
150
100
50
30
20
10
0
0
0.5
1
1.5
2

Fig. 1

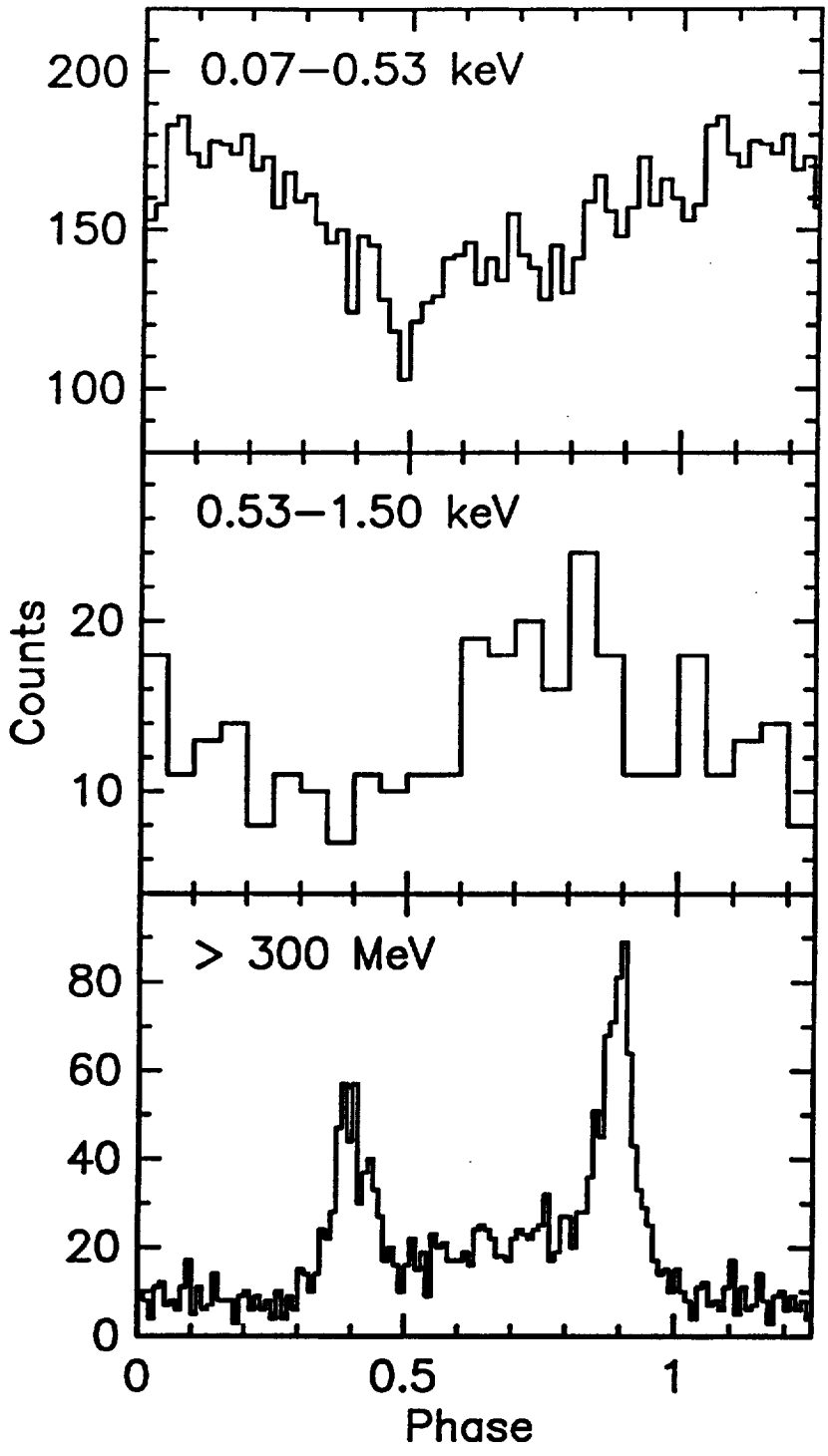
0.07–0.53 keV
0.53–1.50 keV
> 300 MeV
Counts
Phase
200
150
100
20
10
80
60
40
20
0
0
0.5
1

Fig. 2

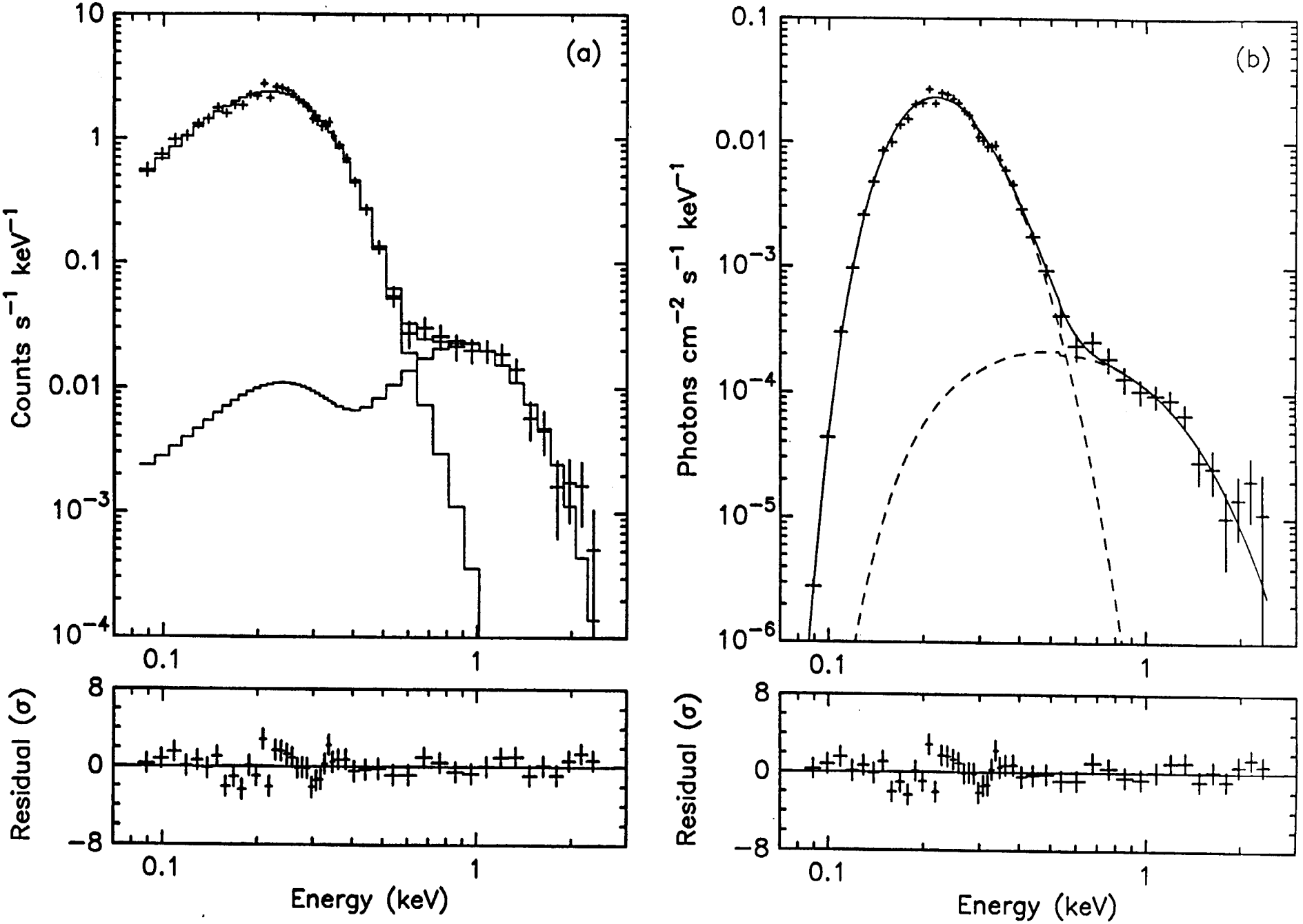
(a)
(b)
Counts s^{-1} keV^{-1}
Photons cm^{-2} s^{-1} keV^{-1}
Residual (σ)
Energy (keV)
10
1
0.1
0.01
10^{-3}
10^{-4}
10^{-5}
10^{-6}
8
0
−8

Fig. 3

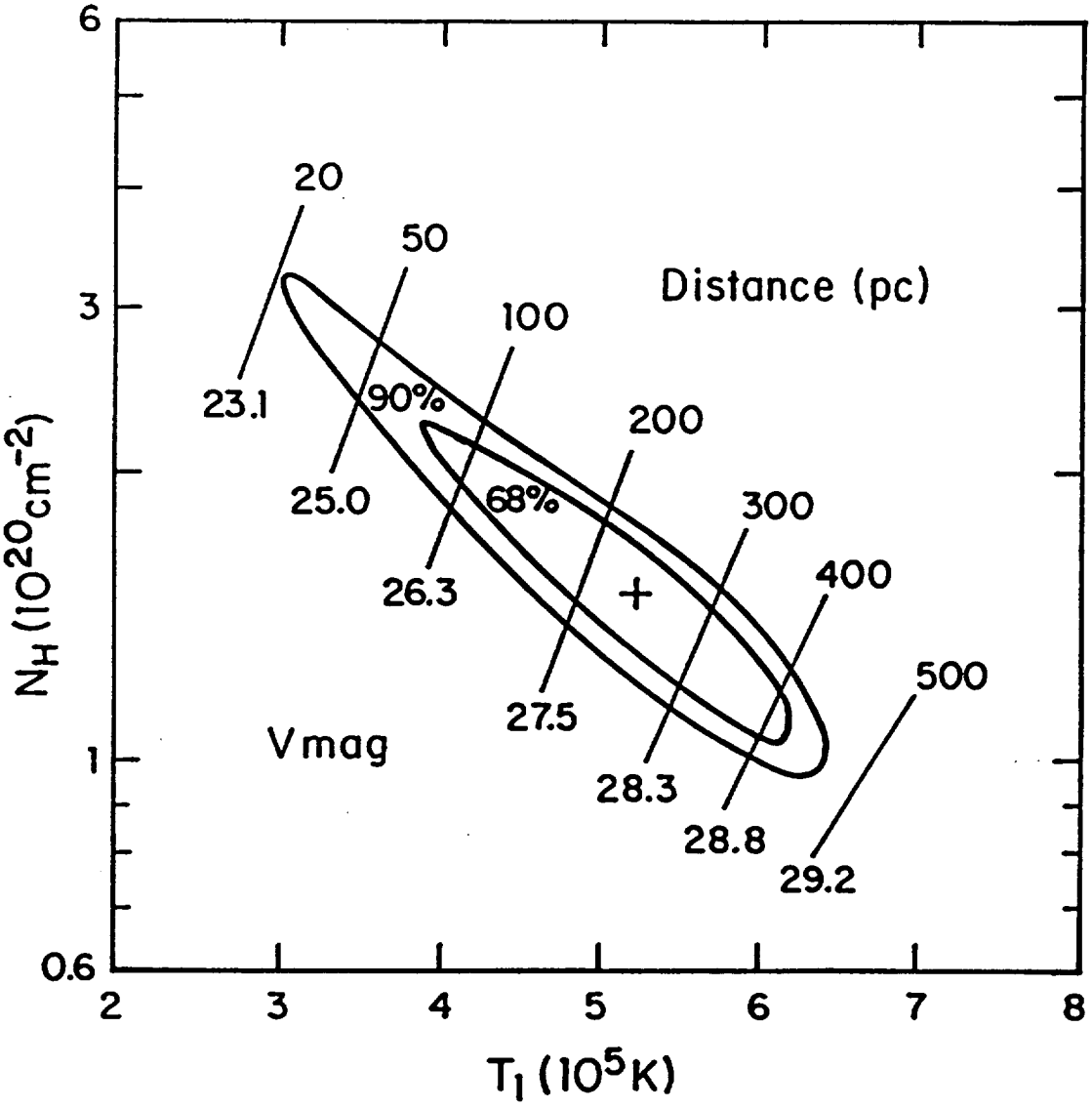

Fig. 4

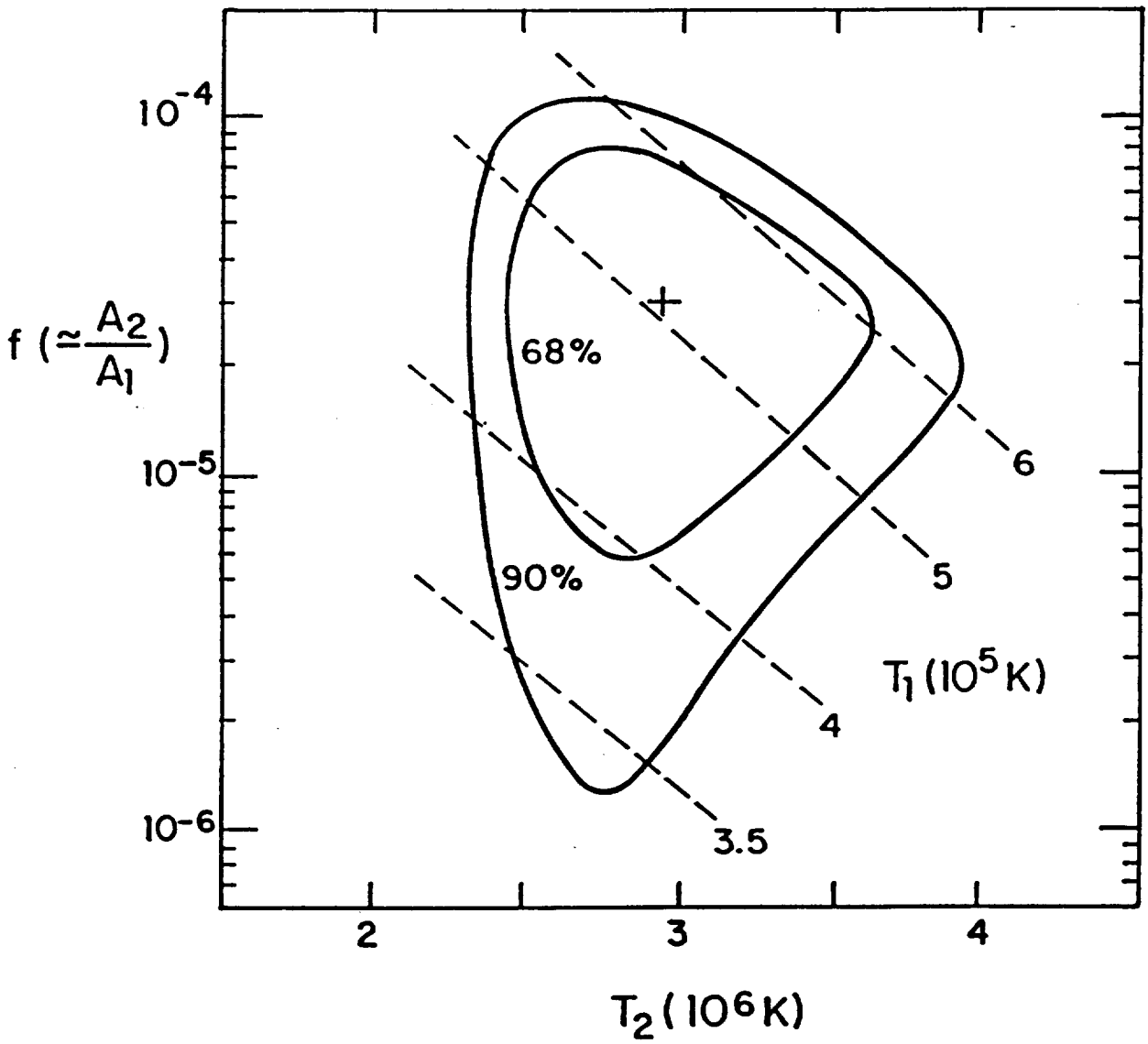

Fig. 5

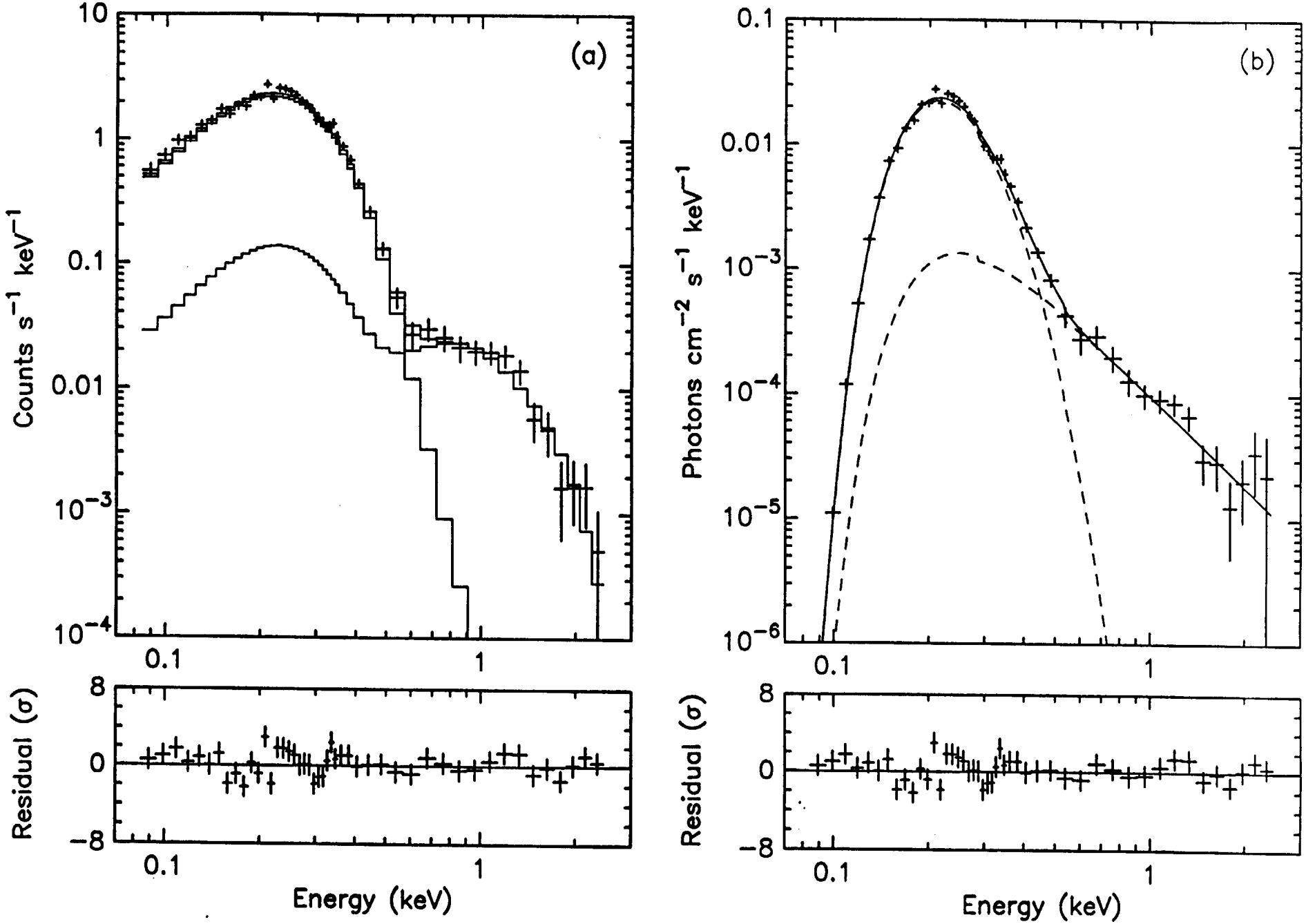
(a)
(b)
Counts s^{-1} keV^{-1}
Photons cm^{-2} s^{-1} keV^{-1}
Residual (σ)
Energy (keV)
10
1
0.1
0.01
10^{-3}
10^{-4}
10^{-5}
10^{-6}
8
0
−8
0.1
1

Fig. 6

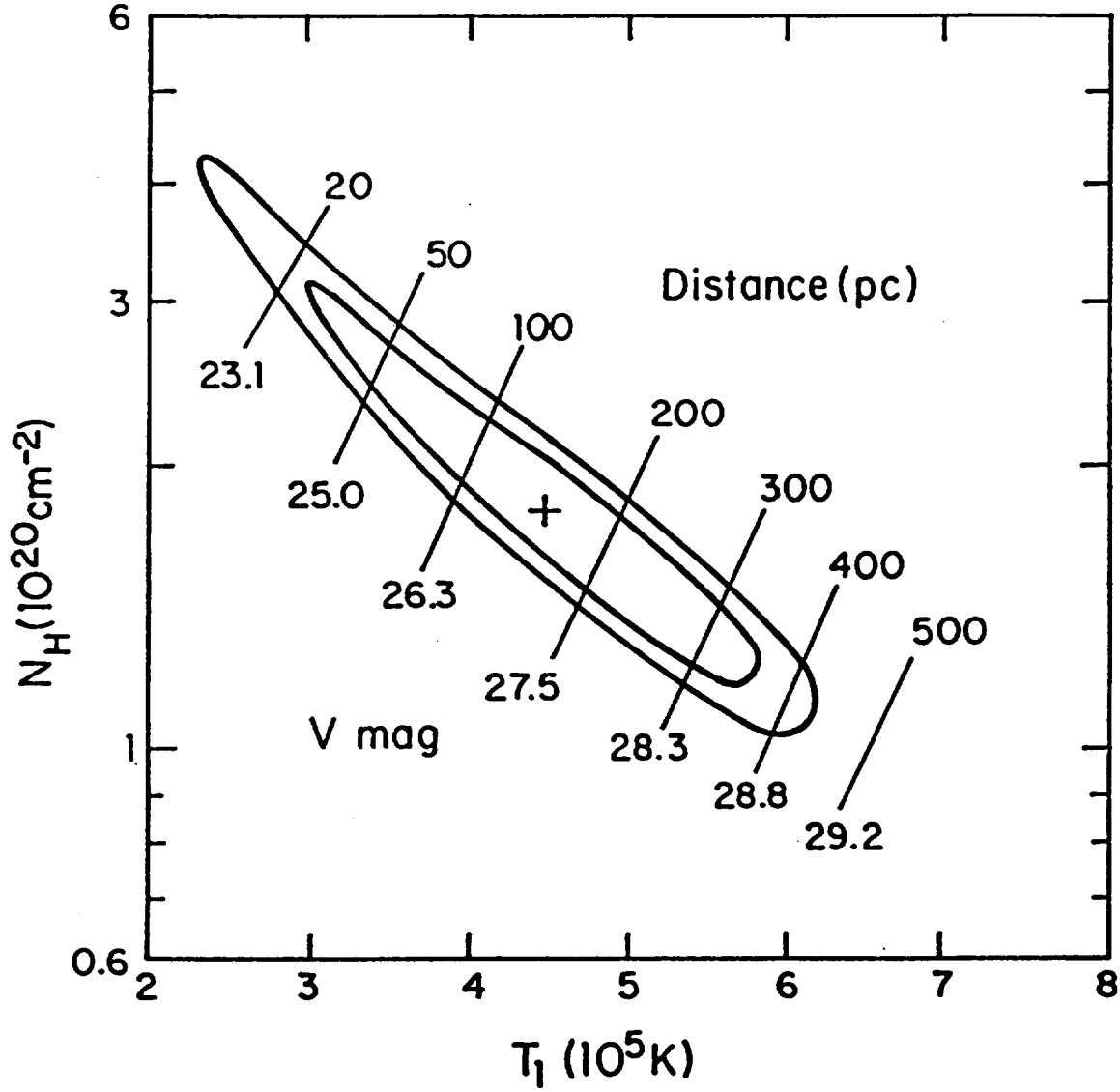

Fig. 7

ORS 0083 HALPERN

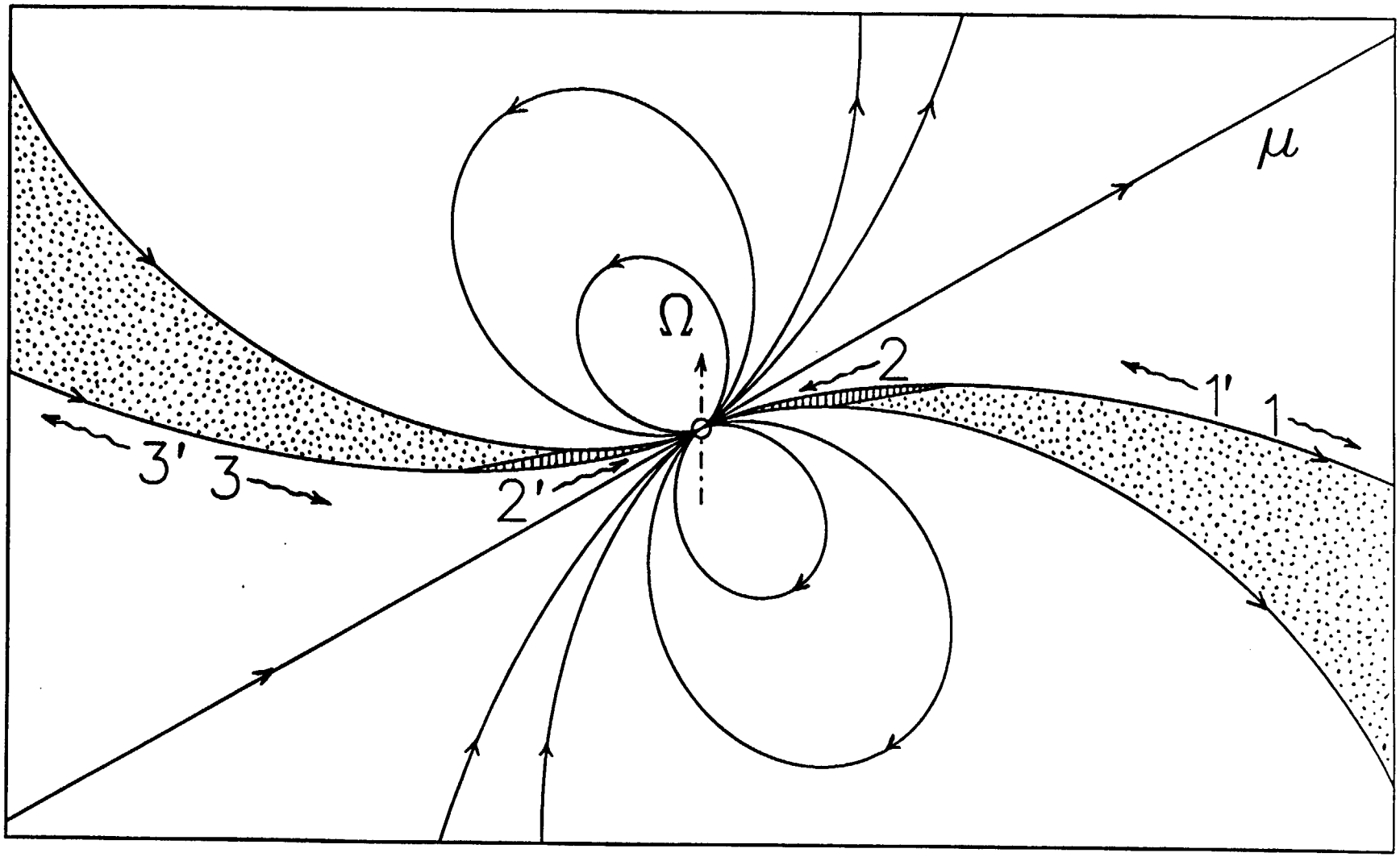

Fig. 8

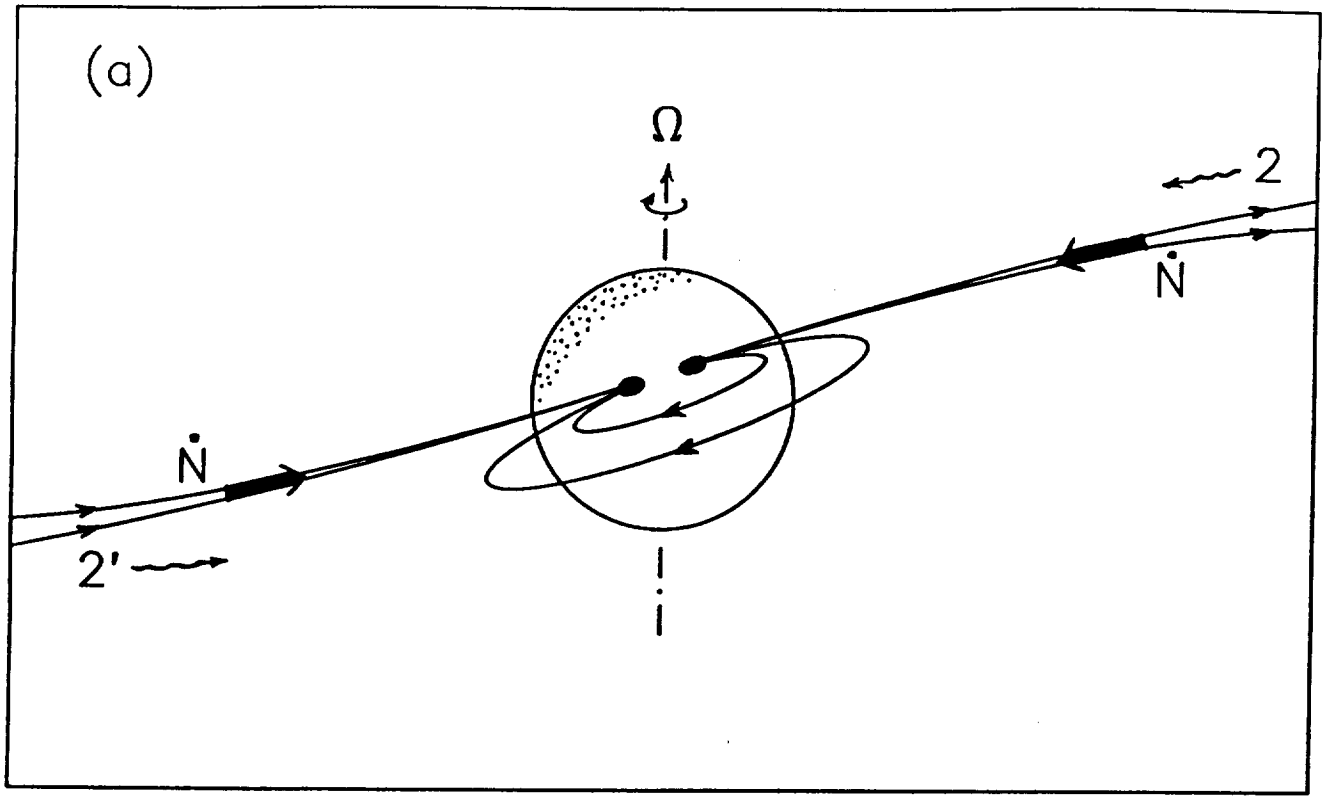

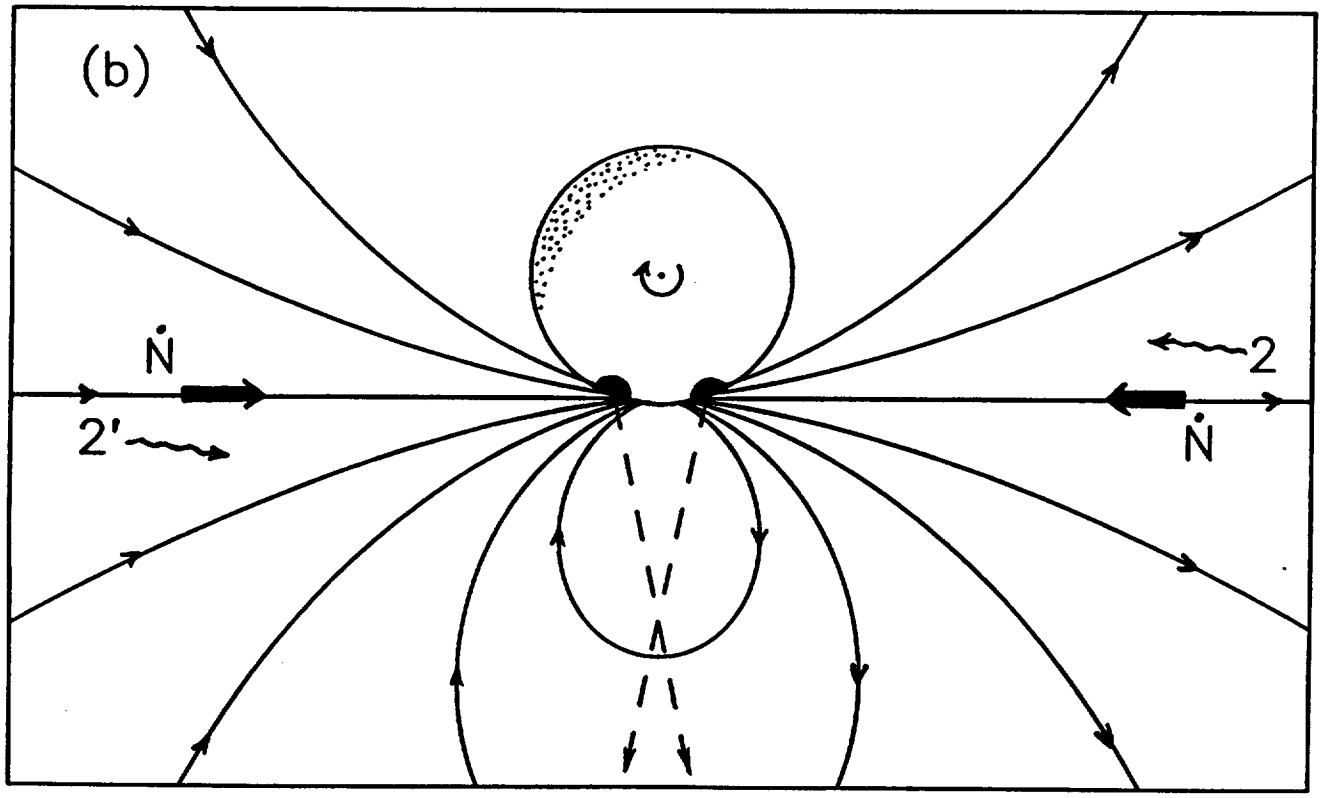

Fig. 9

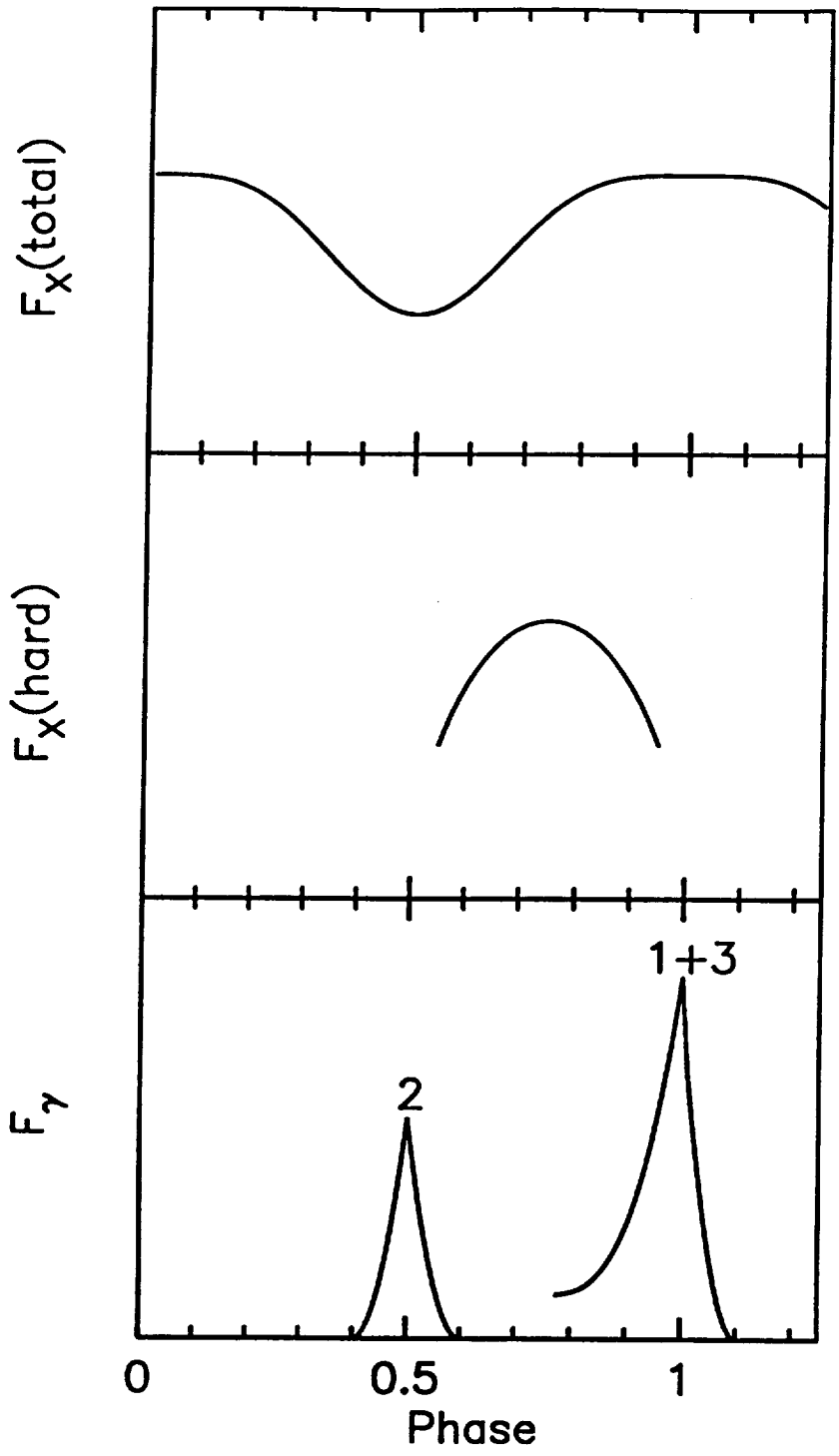

Fig. 10